












RESEARCH ARTICLE

Cocaine perturbs mitovesicle biology in the brain

Pasquale D'Acunzo^{1,2}  | Jonathan M. Ungania¹  | Yohan Kim^{1,2}  |
 Bryana R. Barreto¹  | Steven DeRosa¹ | Monika Pawlik¹  | Stefanie Canals-Baker³ |
 Hediye Erdjument-Bromage^{4,5}  | Audrey Hashim³ | Chris N. Goulbourne¹  |
 Thomas A. Neubert^{4,5}  | Mariko Saito^{2,3}  | Henry Serksen^{2,3}  | Efrat Levy^{1,2,6,7} 

¹Center for Dementia Research, Nathan S. Kline Institute for Psychiatric Research, Orangeburg, New York, USA

²Department of Psychiatry, New York University Grossman School of Medicine, New York, New York, USA

³Division of Neurochemistry, Nathan S. Kline Institute for Psychiatric Research, Orangeburg, New York, USA

⁴Department of Cell Biology, New York University Grossman School of Medicine, New York, New York, USA

⁵Kimmel Center for Biology and Medicine at the Skirball Institute, New York University Grossman School of Medicine, New York, New York, USA

⁶Department of Biochemistry & Molecular Pharmacology, New York University Grossman School of Medicine, New York, New York, USA

⁷NYU Neuroscience Institute, New York University Grossman School of Medicine, New York, New York, USA

Correspondence

Efrat Levy, Center for Dementia Research, Nathan S. Kline Institute for Psychiatric Research, Orangeburg, New York 10962, USA.
 Email: efrat.levy@nki.rfmh.org

Data availability, declaration of interest and funding statements: This work was supported by the National Institute of Health under grants DA044489 to E.L. and M.S., RR027990 to T.A.N., and AG057517 to E.L. The authors report no competing interests. The raw mass spectrometry data generated during this study are available at MassIVE (UCSD, <https://massive.ucsd.edu/ProteoSAFe/static/massive.jsp>) with accession number MSV000089323. The authors confirm that all other data supporting the findings of this study are available within the article and its supplementary material.

Funding information

National Institute on Drug Abuse, Grant/Award Number: DA044489; National Institute of Health Shared Instrumentation Program, Grant/Award Number: S10 RR027990; National Institute on Aging, Grant/Award Number: AG057517

Abstract

Cocaine, an addictive psychostimulant, has a broad mechanism of action, including the induction of a wide range of alterations in brain metabolism and mitochondrial homeostasis. Our group recently identified a subpopulation of non-microvesicular, non-exosomal extracellular vesicles of mitochondrial origin (mitovesicles) and developed a method to isolate mitovesicles from brain parenchyma. We hypothesised that the generation and secretion of mitovesicles is affected by mitochondrial abnormalities induced by chronic cocaine exposure. Mitovesicles from the brain extracellular space of cocaine-administered mice were enlarged and more numerous when compared to controls, supporting a model in which mitovesicle biogenesis is enhanced in the presence of mitochondrial alterations. This interrelationship was confirmed in vitro. Moreover, cocaine affected mitovesicle protein composition, causing a functional alteration in mitovesicle ATP production capacity. These data suggest that mitovesicles are previously unidentified players in the biology of cocaine addiction and that target therapies to fine-tune brain mitovesicle functionality may be beneficial to mitigate the effects of chronic cocaine exposure.

KEYWORDS

cocaine, exosome, extracellular vesicle, microvesicle, mitochondria, mitophagy, mitovesicle

1 | INTRODUCTION

Cocaine is a highly addictive alkaloid extracted from the leaves of the tropical plants of the genus *Erythroxylum*, including *Erythroxylum coca* and *Erythroxylum novogranatense*. The main effects of cocaine in the brain, including euphoria, are mediated by the dopaminergic system (Romach et al., 1999) as cocaine inhibits dopamine reuptake from the extracellular space

This is an open access article under the terms of the [Creative Commons Attribution-NonCommercial-NoDerivs](https://creativecommons.org/licenses/by-nc-nd/4.0/) License, which permits use and distribution in any medium, provided the original work is properly cited, the use is non-commercial and no modifications or adaptations are made.

© 2023 The Authors. *Journal of Extracellular Vesicles* published by Wiley Periodicals, LLC on behalf of the International Society for Extracellular Vesicles.

through high-affinity binding to the presynaptic dopamine transporter (known as SLC6A3 or DAT), resulting in the elevation of dopamine extracellular levels. Nonetheless, cocaine activity is complex and includes several pan-neuronal, non-dopaminergic changes, including global alterations in brain metabolism and well-established perturbations of mitochondrial homeostasis, especially after chronic exposure (Thornton et al., 2021). In a study involving only male subjects, cocaine use reduced glucose brain metabolism in 26 out of 29 brain regions (London et al., 1990), an effect that persisted at least 4 months after cocaine detoxification (Volkow et al., 1992). In vitro, primary cortical neurones exposed to cocaine show reduced ATP production and decreased mitochondrial potential (Cunha-Oliveira et al., 2006; Cunha-Oliveira et al., 2010; De Simone et al., 2016). Other studies confirmed that the reduction in ATP, at least in part, is a direct effect of the drug on mitochondria rather than a consequence of perturbed cellular dynamics (Cunha-Oliveira et al., 2013a, 2013b; Yuan & Acosta, 2000; Lehmann et al., 2003; Zhou et al., 2011; Bhattacharjee et al., 2019; Dietrich et al., 2004). Mitochondria purified from rat liver, heart, and brain tissues and incubated in vitro with cocaine manifest suppression of mitochondrial energy production and oxygen consumption, likely via a direct block of the electron transport chain (ETC) complex I enzymatic activity (Cunha-Oliveira et al., 2013a, 2013b; Yuan & Acosta, 2000). The involvement of cocaine in mitochondrial homeostasis was further corroborated by analyses of expression of brain ETC genes after cocaine use or administration in humans and rodents, respectively (Bhattacharjee et al., 2019; Dietrich et al., 2004; Lehmann et al., 2003; Zhou et al., 2011). A single dose of cocaine is sufficient to specifically downregulate rat cortical ETC complex I subunits encoded by mitochondrial DNA (mtDNA) (Dietrich et al., 2004), reinforcing the idea that cocaine is actively imported into the mitochondrial matrix where it interferes with mtDNA expression. Moreover, nuclear RNA seq-based gene expression studies in the hippocampus of individuals with either cocaine or alcohol use disorder demonstrated that the downregulation of ETC complex I genes, including *Ndufa5*, is cocaine-specific and not found in the brain of people with alcohol use disorder (Zhou et al., 2011).

Given the profound impact of cocaine on mitochondrial homeostasis after prolonged exposure, we hypothesised that the cocaine-induced mitochondrial damage reverberates in an altered biogenesis and release of mitovesicles, a previously unappreciated subset of small extracellular vesicles (EVs) of mitochondrial origin that we identified for the first time in the brain extracellular space and that we recently characterised in detail (D'Acunzo et al., 2021). Mitovesicles are unique entities when compared to the two other known EV subpopulations, exosomes and microvesicles, and to intracellular mitochondria. Unlike exosomes and microvesicles, mitovesicles are characterised by: (I) specific biophysical and biochemical properties, including a higher density and a higher protein/lipid ratio; (II) the presence of a double membrane and an electron-dense core when visualised by cryogenic electron microscopy (cryo-EM); (III) the lack of microvesicle- and exosome-specific proteins; (IV) a specific lipidome, including the enrichment of the mitochondrial lipid cardiolipin; (V) the incorporation of mitochondria-specific dyes (e.g., MitoTracker); and (VI) the ability to produce ATP via ETC in vitro (D'Acunzo et al., 2021; D'Acunzo et al., 2022). Mitovesicles are also distinguishable from microvesicles by their smaller size (D'Acunzo et al., 2021; D'Acunzo et al., 2022), while the hydrodynamic diameters of mitovesicles and exosomes largely overlap when studied by nanoparticle tracking analysis (NTA) (D'Acunzo et al., 2021; D'Acunzo et al., 2022). However, mitovesicles are distinctively characterised by a double membrane and an electron-dense core under cryo-EM, while exosomes and microvesicles are surrounded by a single membrane and display a more electron-lucent lumen (D'Acunzo et al., 2021). In addition, cryo-EM shows that mitovesicles differ substantially from their organelle of origin, given their smaller size (100–300 nm vs. 500–2000 nm of intracellular mitochondria), a narrower intermembrane space (IS) and the absence of *cristae* (D'Acunzo et al., 2021). Moreover, mass spectrometry and Western blot analyses demonstrated that only a specific subset of catabolic mitochondrial proteins is found in mitovesicles. Several mitochondrial components, although abundant in intracellular mitochondria and in degradative intracellular vesicles of mitochondrial origin (known as mitochondrial-derived vesicles or MDVs), are absent in the extracellular mitovesicle proteome, including—but not limited to—TOMM20 and Mitofusin-2 (MFN2) (D'Acunzo et al., 2021; D'Acunzo et al., 2022; Sugiura et al., 2014). The absence of TOMM20 in mitovesicles and its presence in intracellular mitochondria and in the majority of MDVs were later confirmed by another group studying mitovesicle responses in brown adipose tissue upon thermic mitochondrial stressors, both in vitro and in vivo (Rosina et al., 2022).

We have previously shown that chronic cocaine exposure alters the levels and cargo of exosomes in a sex-dependent fashion (Barreto et al., 2022; Landfield et al., 2021). In addition, we (D'Acunzo et al., 2021) and others (Rosina et al., 2022) showed higher secretion of mitovesicles into the extracellular space under conditions with mitochondrial damage, likely a compensatory mechanism to avoid the accumulation of toxic and oxidised mitochondrial components within the cell. Thus, we investigated intracellular levels of proteins involved in mitochondrial dynamics and the size, levels, and cargo of extracellular mitovesicles in the brain of both male and female mice after chronic, non-contingent cocaine treatments. We demonstrate that all these parameters are altered by cocaine, and that mitovesicle cargo loading and functionality are perturbed in male but not in female cocaine-treated mice.

This study reveals that mitovesicles are a previously unidentified player in the biology of chronic cocaine exposure in the brain, and that mitovesicle alterations may contribute to metabolic responses to addictive drugs.

2 | MATERIALS AND METHODS

2.1 | Experimental design and statistical analyses

For non-contingent chronic cocaine exposure, 2.5-month-old male and female C57BL/6J mice (RRID:IMSR_JAX:000664, Jackson Laboratory, Bar Harbor, ME, US) were intraperitoneally injected once daily for 12 days with either 0.9% NaCl (hereafter saline, Hospira, Lake Forest, IL, US) as a control or cocaine-HCl dissolved in saline (Sigma-Aldrich, St. Louis, MO, US), 10 mg per kg body weight. This dosage is sufficient to generate sex-specific behavioural responses to cocaine at the end of the treatment, as measured by total ambulatory counts (Barreto et al., 2022; Reith et al., 2012). Mice were sacrificed by cervical dislocation 30 min after the final cocaine/saline injection, the brains quickly removed, and the two hemibrains (without the cerebellum, the brainstem, and the olfactory bulbs) frozen at -80°C until further processing.

All experiments were performed following the 'Animal Research: Reporting In Vivo Experiments' (ARRIVE) guidelines. Mice were randomly allocated to saline or cocaine groups. Likewise, cage location and the order of treatments were randomly assigned. The EV characterisation reported in this work is designed to comply with the MISEV2018 guidelines (Thery et al., 2018). In each experiment, EVs were isolated simultaneously from one hemibrain from each experimental group (male treated with saline, male treated with cocaine, female treated with saline, female treated with cocaine). Accordingly, isolations were performed on four samples at a time. Given a left/right hemibrain asymmetry in metabolic responses to cocaine (Volkow et al., 1999), EVs were always isolated from the right hemibrain, as previously described (D'Acunzo et al., 2022). The number of mice included in each experimental group is reported in all figure legends as the variable n . No criteria have been set to exclude animals and/or data points—thus, no datapoints were excluded from any of the analyses. Changes were considered significant when $P < 0.05$ (95% confidence interval). Statistical analyses were carried out using GraphPad Prism (version 6.01, GraphPad Holdings, San Diego, CA, US).

Mitovesicle and total EV diameters were estimated using cryo-EM (Figure 1c) and NTA (Figures 1d and 5h), showing a similar positive skewness in the relative size distributions. This was an expected outcome as both techniques tend to overestimate the proportion of bigger EVs and not count or lose part of the smaller ones, consistent with previous reports from our group (D'Acunzo et al., 2021) and others (Linares et al., 2017). Morphological descriptors of Neuro-2a cell mitochondria, including area and perimeter, were estimated using the software ImageJ (National Institute of Health, Bethesda, MD, US) (Schneider et al., 2012), as previously described (Wiemerslage & Lee, 2016). In particular, we considered the perimeter-to-area ratio (also known as 'mitochondria interconnectivity index', 'branching index', or 'form factor') (Picard et al., 2013; Wiemerslage & Lee, 2016) as an indicator of mitochondria morphology, as previously extensively discussed and described (Picard et al., 2013; Wiemerslage & Lee, 2016). In short, it can be geometrically demonstrated that a circle (ideally, the shape of fully fragmented mitochondria) has the minimal perimeter possible for a given area (low branching index), while the perimeter-to-area ratio rises with increasing frequency of concavity (high branching index) which are typically found in a network of fused mitochondria. Both mitochondrial area (Figure 5b) and branching index (Figure 5c) had a positive skewness, similar to cryo-EM and NTA data of EVs. This was expected as fused mitochondria can be several μm long, while fragmented mitochondria cannot be smaller than a certain threshold. For these reasons, significance was calculated using the Mann-Whitney U test for cryo-EM data in Figure 1c and for mitochondria descriptors in Figure 5b,c, while statistics of the NTA data was performed using a binning system (Figure 1e), as previously reported elsewhere in detail (D'Acunzo et al., 2019; D'Acunzo et al., 2021). For Figure 1e, the statistical analysis was performed through two-way ANOVA (variables: treatment; size bin) followed by post-hoc Bonferroni's multiple comparisons test. The total number of mitovesicles analyzed under cryo-EM was 90 for the saline group and 143 for the cocaine group, respectively, while the total number of Neuro-2a mitochondria analyzed was 134 for the saline group and 161 for the cocaine group, respectively.

For densitometry quantification of protein bands, we used the software ImageJ. All histograms were plotted as mean \pm standard error of the mean (SEM). To improve clarity of the data, all datapoints are provided for each experiment, shown as smaller dots superimposed on the relative graph. For in vivo experiments, each datapoint corresponds to the data derived from a separate mouse. Significance was calculated by two-way ANOVA (variables: treatment; sex) with post-hoc Bonferroni's multiple comparisons test. For in vitro experiments, each datapoint corresponds to a different EV isolation and/or independent replicate of the experiment with a different batch of cells, for example, cells after different days in vitro/passage numbers. When two groups were compared, significance was calculated using either the Student's t -test or the Mann-Whitney U test in case of distributions that were unequivocally found to be non-normal (as in Figure 5b,c), as described above.

For nanoflow liquid chromatography-mass spectrometry (LC-MS/MS), all data were analyzed using MaxQuant proteomics software (version 1.5.5.1) with the Andromeda search engine (Cox et al., 2011) using a murine database (*Mus musculus* protein database; Uniprot; Reviewed, 16,950 entries, [12202017]). Reporter ion mass tolerance was set to 0.01 D, the activated precursor intensity fraction value was set to 0.75, and the false discovery rate was set to 1% for protein, peptide-spectrum match, and site decoy fraction levels. Peptides were required to have a minimum length of seven amino acids and a mass no greater than 4,600 Da. The reporter ion intensities were defined as intensities multiplied by injection time (to obtain the total signal) for

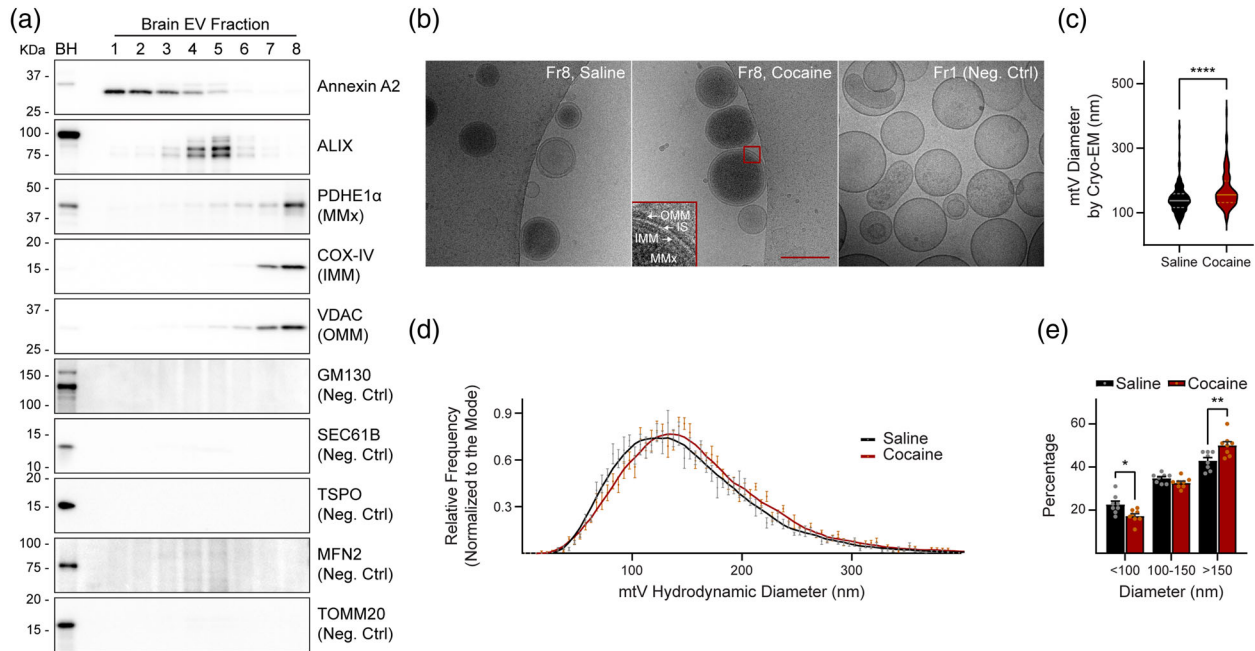


FIGURE 1 Mitovesicles isolated from the brain of cocaine-treated mice are larger than mitovesicles from saline-treated controls. (a) Representative Western blot analyses of EVs isolated from the right hemibrain of a 3-month-old C57BL/6J male mouse and fractionated using a high-resolution OptiPrep density step-gradient. The left hemibrain of the same mouse was homogenised and loaded in the first lane as a control to check the relative abundance of a specific protein in EVs as compared to brain homogenate (BH). The same volume (5 µl) of each sample was loaded into each lane. Annexin A2 is a marker of microvesicles, ALIX a marker of exosomes, and PDHE1α, COX-IV, and VDAC are markers of the mitovesicle matrix (MMx), the inner mitovesicle membrane (IMM), and the outer mitovesicle membrane (OMM), respectively. Unrelated intracellular compartments (assessed by the Golgi marker GM130 and the endoplasmic reticulum marker SEC61B) and potential intracellular mitovesicle contaminant such as MDVs and whole mitochondria (assessed by MFN2, TSPO, and TOMM20), were undetectable in brain EV fractions but abundantly found in BH. KDa: kilodaltons. Uncropped, unprocessed blots are available in Suppl. Figure 1. (b) Representative photomicrographs of fraction 8 (Fr8) EVs imaged under cryo-EM and isolated from the right hemibrain of either saline- or cocaine-treated mice. As a control, fraction 1 (Fr1) EVs (saline-treatment) are also shown. Mitovesicles, characterised by the presence of a double membrane and an electron dense matrix (red box inset), were enriched in Fr8 EVs in both saline- and cocaine-treated brains but not in Fr1 EVs. MMx: mitovesicle matrix. IMM: inner mitovesicle membrane. IS: intermembrane space. OMM: outer mitovesicle membrane. Red box (lower left): area magnified in the red inset. Scale bar: 200 nm. (c) Diameter distribution of Fr8 mitovesicles (mtVs) isolated from the right hemibrain of either saline- or cocaine-treated mice and imaged under cryo-EM (violin plot). Number of total photomicrographs analyzed per group: 45, for a total of 90 mitovesicles for the saline- and 143 mitovesicles for the cocaine group, respectively. Statistical test: Mann-Whitney *U* test. *****P* < 0.0001. (d) Hydrodynamic diameter distribution of Fr8 mitovesicles (mtVs) isolated from the right hemibrain of either saline- or cocaine-treated mice, as assessed by NTA. Both sexes were combined as we did not see any appreciable sex-difference in the mitovesicle hydrodynamic size. The distributions were normalised to the mode, while the bell curves were obtained using a seven-point moving average. *n* = 8 mice per group. (e) Hydrodynamic size analysis of Fr8 mitovesicles isolated from the right hemibrain of either saline- or cocaine-treated mice, as estimated by NTA. Data were grouped in three size bins (bin 1: < 100 nm; bin 2: 100–150 nm; bin 3: > 150 nm) and plotted as the percentage of mitovesicles in each mouse with a diameter that falls within one of these bins. Both sexes were combined as we did not see any appreciable sex-difference in the mitovesicle hydrodynamic size. Bars represent mean ± SEM. *n* = 8 mice per group. Statistical test: two-way ANOVA (variables: treatment; size bin) with Bonferroni's multiple comparisons test. **P* < 0.05, ***P* < 0.01

each isobaric labelling channel summed over all MS/MS spectra, as previously validated (Tyanova, Temu, & Cox, 2016). We also performed separate analyses of unlabelled peptides by using the same LC-MS/MS method. Mass spectra were analyzed by label-free quantitation using MaxQuant (version 1.5.5.1) with the Andromeda search engine (Cox et al., 2011; Tyanova, Temu, Sinitcyn, et al., 2016) and Perseus (version 1.5.6.0) (Tyanova, Temu, Sinitcyn, et al., 2016). The results of the *t*-test between cocaine and control groups were displayed in a volcano plot and significant data points were determined with a permutation-based FDR calculation based on the Benjamini-Hochberg procedure (Figure 2a).

2.2 | Cell line and culturing conditions

Murine male neuroblastoma Neuro-2a cells (ATCC Cat# CCL-131, RRID:CVCL_0470) and human female neuroblastoma SH-SY5Y cells (ATCC Cat# CRL-2266, RRID:CVCL_0019) were purchased from the American-Type Culture Collection (ATCC, Manassas, VA, US) and grown at 37°C in Dulbecco's modified Eagle's medium (DMEM), supplemented with 10% *v/v* heat-inactivated fetal bovine serum and 2 mM GlutaMAX (all reagents from Thermo Fisher Scientific, Waltham, MA, US) at 5% CO₂ in a humidified incubator. As streptomycin inhibits mitoribosomes and alters mitochondria functionality (Wang et al., 2015), the

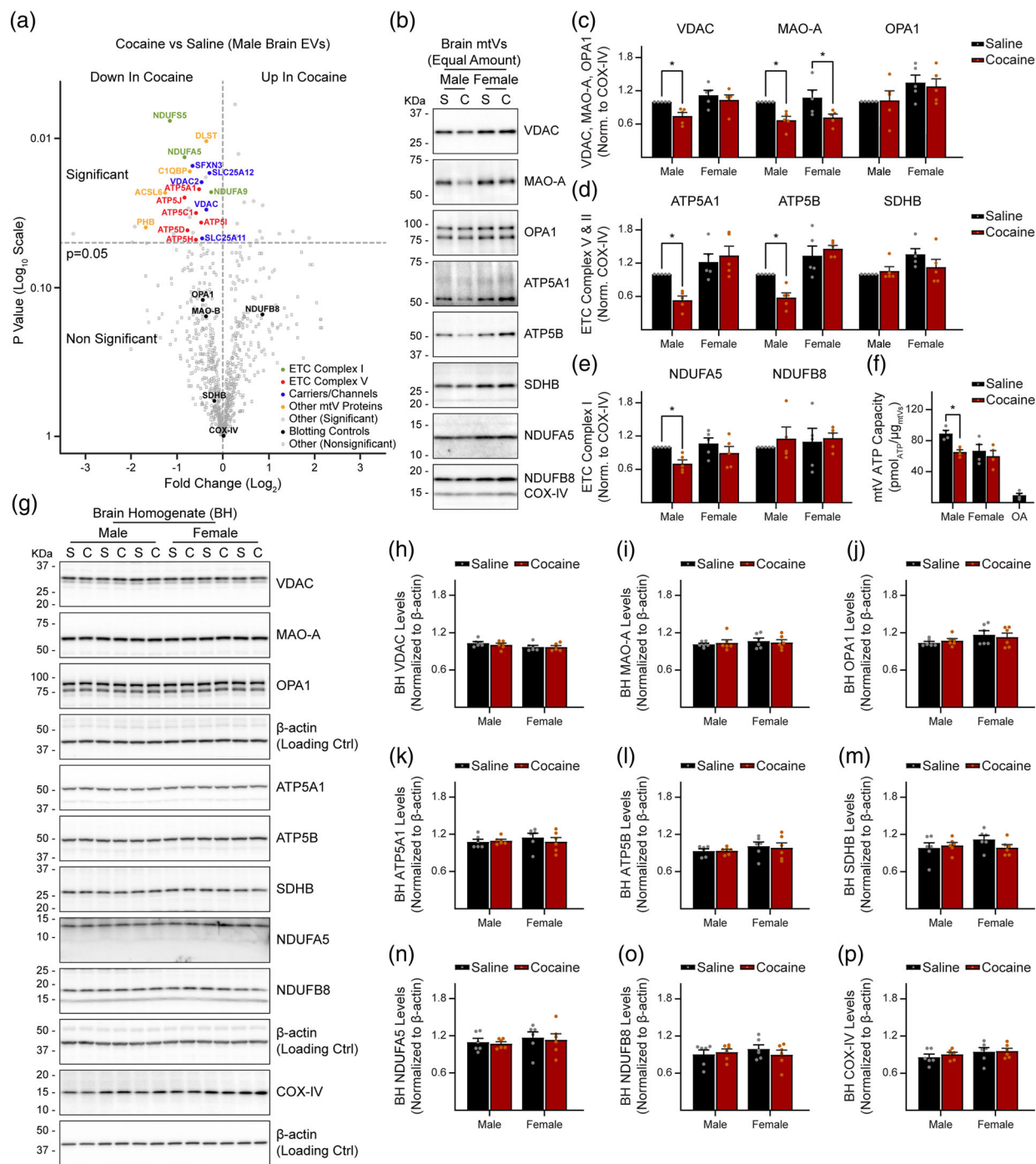


FIGURE 2 Cocaine alters brain mitovesicle cargo and functionality. (a) LC-MS/MS analysis of EV proteins (all fractions combined) isolated from the right hemibrain of either saline- or cocaine-treated male mice (volcano plot). Equal amounts of EV proteins were analyzed (10 μg , as estimated by the BCA assay for total protein content). Significance was set at $P < 0.05$ (the demarcation line is shown). Mitovesicle proteins that are significantly different between saline- and cocaine-treated male mice are spelled out and coloured, as follows: green, ETC Complex I subunits; red, ETC Complex V subunits; blue: mitochondria/mitovesicle-specific carriers for small molecules and mitochondria/mitovesicle ion channels; yellow: mitovesicle proteins with miscellaneous functions. Mitovesicle proteins that did not change significantly between the groups and therefore were used as controls in subsequent Western blot analyses are in black. Other non-mitovesicle proteins that were significantly different between the experimental groups are in grey, while nonsignificant changes are shown as empty grey squares. $n = 3$ mice per group. The full list of identified proteins is provided in Suppl. Table 1. Quality control data are available in Suppl. Figure 6. (b) Representative Western blot analyses of equal protein amounts of Fr8 mitovesicles (mtVs) isolated from the right hemibrain of either saline- or cocaine-treated male or female mice. The isolation was performed on four samples at a time, one for each experimental group. 0.5 μg of mitovesicle proteins were loaded in each lane, as estimated by the BCA assay for total protein content. KDa: kilodaltons. Uncropped, unprocessed blots are available in Suppl. Figure 2a. (c–e) Densitometric quantifications of the bands corresponding to the proteins VDAC, MAO-A, OPA1 (c), the ETC Complex V subunits ATP5A1 and ATP5B, the ETC Complex II subunit SDHB (d), and the ETC Complex I subunits NDUF5 and NDUF8 (e) in mitovesicle lysates analyzed by Western blot, as specified in (b). The ETC Complex IV subunit COX-IV was used as the loading control. Graphs are plotted as a fold change over the saline-injected male

(Continues)

FIGURE 2 (Continued)

within each isolation. Bars represent mean \pm SEM. $n = 5$ mice per group. Statistical test: two-way ANOVA (variables: treatment; sex) with Bonferroni's multiple comparisons test. $*P < 0.05$. (f) Analysis of the ATP production capacity of mitovesicles (mtVs) isolated from the right hemibrain of either saline- or cocaine-treated male or female mice. As a control, the sample from the saline-injected male of each isolation was treated in parallel with the ETC Complex III and V inhibitors oligomycin and antimycin-A (OA). Mitovesicle ATP capacity was calculated as the difference in the levels of ATP (expressed as pmol) after incubation of mitovesicles with substrates to boost oxidative phosphorylation (malate, pyruvate, ADP, Mg^{2+}) for 10 min at 37°C minus the basal ATP levels at time 0, normalised to the amount of mitovesicles (expressed in μg). Bars represent mean \pm SEM. $n = 4$ mice per group. Statistical test: two-way ANOVA (variables: treatment; sex) with Bonferroni's multiple comparisons test. $*P < 0.05$. (g) Representative Western blot analyses after loading equal amounts (10 μg , as estimated by BCA assay) of brain homogenates (BH) from either saline- or cocaine-treated male or female mice. Three different mice per experimental group are shown. Homogenisation was performed for all samples at the same time. S: saline-treated mouse; C: cocaine-treated mouse. kDa: kilodaltons. Uncropped, unprocessed blots are available in Suppl. Figure 2b. (h–p) Densitometric quantifications of the bands corresponding to the proteins VDAC (h), MAO-A (i), OPA1 (j), the ETC Complex V subunits ATP5A1 (k) and ATP5B (l), the ETC Complex II subunit SDHB (m), the ETC Complex I subunits NDUFA5 (n) and NDUFB8 (o), and the ETC Complex IV subunit COX-IV (p) in brain homogenates (BH) analyzed by Western blot, as specified in (g). β -actin was used as the loading control. Graphs are plotted as a fold change over the first lane of the set (saline-injected male). Bars represent mean \pm SEM. $n = 6$ mice per group. Statistical test: two-way ANOVA (variables: treatment; sex) with Bonferroni's multiple comparisons test

penicillin (100 U/ml) + streptomycin (100 μg /ml) supplement from Thermo Fisher Scientific (PenStrep) usually used to limit bacterial growth was not added to the cell culture medium. Instead, bacterial and mycoplasma contaminations were routinely checked by staining with 4',6-diamidino-2-phenylindole (DAPI, Thermo Fisher Scientific) of a spared aliquot of cells in use after passage. The presence of extranuclear DAPI signal was considered as an indication of the presence of extranuclear DNA and as a contamination. In case of contamination, cells were eliminated, and a new contamination-free cell stock thawed to restart the line. Cell viability was evaluated by 0.4% w/v Trypan Blue (Sigma-Aldrich) staining (1:1 v/v dye-to-cell ratio) of an aliquot of the cells in use. Positive (dead) cells were counted using a haemocytometer under a microscope following standard procedures. To avoid cellular senescence and the accumulation of DNA replication errors, experiments were performed using cells at not higher passage than #16 (starting from frozen stocks at passage #4 for Neuro-2a and passage #3 for SH-SY5Y cells).

2.3 | Brain homogenisation

Total protein levels were analyzed in left hemibrains after homogenisation. Briefly, brain tissues were homogenised in 10:1 v/w tissue homogenisation buffer (0.25 M sucrose, 20 mM Tris-HCl pH 7.4, 1 mM EDTA, 1 mM EGTA; all reagents from Sigma-Aldrich) supplemented with protease inhibitors (5 μg /ml leupeptin, 5 μg /ml antipain dihydrochloride, 5 μg /ml pepstatin A, 1 mM phenylmethanesulfonyl fluoride, 1 μM E64; all reagents from Sigma-Aldrich) immediately before homogenisation. The procedure was performed in ice-cold glass homogenizers with 20 complete strokes of Teflon pestles (Wheaton, DWK Life Sciences, Millville, NJ, US). Aliquots of homogenate were stored at -80°C until use.

2.4 | Isolation of mitovesicles from the brain extracellular space

Murine brain mitovesicles were isolated from right hemibrains as described in detail in our most recent protocol paper (D'Acunzo et al., 2022). In short, after a 15-min treatment with 20 U/ml papain (Worthington, Lakewood, NJ, US) at 37°C, the hemibrain preparation was centrifuged at 300 g for 10 min at 4°C, then filtered using 0.2 μm cellulose acetate syringe filters (Cat# 431219, Corning Inc., Corning, NY, US). The cleared mixture was differentially centrifuged at 2,000 g for 10 min at 4°C and at 10,000 g for 30 min at 4°C to eliminate undigested material and cellular debris. The resulting supernatant was ultra-centrifuged at 100,000 g (k -factor: 207.5, 45Ti rotor type, Beckman Coulter, Brea, CA, US) for 70 min at 4°C to obtain a crude brain EV pellet. Mitovesicles were separated from other small EVs and contaminant using a high-resolution iodixanol step-gradient approach (D'Acunzo et al., 2021; D'Acunzo et al., 2022; Y. Zhang et al., 2021) through which mitovesicles were enriched in the fraction number 8 (Fr8) of the gradient (Figure 1a). Although the secretion of both nude mitochondria and mitochondria-encapsulated microvesicles into the extracellular space was reported before, at least in vitro (Puhm et al., 2019), the strategy employed in this study to isolate brain mitovesicles was designed to separate and pellet these particles out from the other types of EVs. Therefore, both intracellular and extracellular mitochondria components did not contaminate our mitovesicle-enriched pellet—see Figure 1a and D'Acunzo et al., 2021; D'Acunzo et al., 2022.

2.5 | Isolation of EVs from conditioned media and cell lysis

Neuro-2a cells at approximatively 80% confluency in 150-mm tissue culture plates (Corning Inc.) were treated for 24 h either with 1 mM cocaine dissolved in saline or with an equivalent volume of saline (control) in Opti-MEM (Thermo Fisher Scientific), an EV- and serum-free optimised cell medium. This dose of cocaine is known to stimulate mitochondrial dysfunction in the

absence of cell death (Cunha-Oliveira et al., 2010), as also confirmed by our data (Figure 5). Furthermore, Neuro-2a cells are known to grow well in Opti-MEM without addition of serum (Li et al., 2015).

Upon treatments, cells were washed once in PBS and lysed in RIPA buffer (formulation as described; D'Acunzo et al., 2022) supplemented with protease inhibitors (5 μ g/ml leupeptin, 5 μ g/ml antipain dihydrochloride, 5 μ g/ml pepstatin A, 1 mM phenyl-methanesulfonyl fluoride, 1 μ M E64; all reagents from Sigma-Aldrich), while the medium was collected and serially centrifuged at 300 g for 10 min at 4°C, at 2,000 g for 10 min at 4°C, and at 10,000 g for 30 min at 4°C. The resulting supernatant was ultracentrifuged at 100,000 g (36,000 rpm) for 70 min at 4°C in a 45Ti rotor type (Beckman Coulter) to obtain a crude EV pellet, which was later washed in phosphate-buffered saline (PBS, Sigma-Aldrich) and centrifuged again at 100,000 g (50,000 rpm) for 70 min at 4°C in a TLA-55 rotor type (*k*-factor: 79.9, Beckman Coulter). Washed EVs were either resuspended in PBS for NTA or lysed in RIPA buffer for Western blot analysis. In our experimental conditions, EVs isolated from conditioned cell media had a purity index of $5.44 \pm 0.51 \times 10^9$ (mean \pm SEM) particles/ μ g recovered proteins, as estimated in 6 independent isolations by NTA for the particle number and the bicinchoninic acid (BCA, Pierce, Thermo Fisher Scientific) assay for total protein content, respectively.

2.6 | Western blot analysis

Murine brain mitovesicles were analyzed by Western blotting as previously described in detail (D'Acunzo et al., 2022). For the mitovesicle cargo analysis, equal protein amounts were loaded on 4%–20% Tris-HCl gels, as estimated by BCA assay for total protein content. COX-IV was used as a loading control, as its amount was found unchanged between samples in a prior mass spectrometry analysis (see Figure 2a). To investigate the number of mitovesicles (Figure 3a–e), as well as the secretion of different EV subtypes in vitro (Figure 5l,m), equal volumes (5 μ l) of EVs were loaded and the relative densitometric quantifications were normalised to the weight of the brain tissue or to the amount of cells (expressed as μ g of cell lysate) from which the EVs were isolated. The brain homogenate (BH) analyses (Figure 4), as well as cell lysate analyses (Figure 5g), were performed on equal protein amounts (either 5 or 1 μ g, respectively), as estimated by the BCA assay, and normalised to β -actin or to the most appropriate loading control, including the respective total protein in the case of phospho-proteins. The primary antibodies used are listed in Suppl. Table 2. The secondary antibodies (HRP-conjugated) were from Jackson ImmunoResearch (West Grove, PA, US). The chemiluminescent substrate was either ECL or femto ECL (both from Pierce, Thermo Fisher Scientific) for either strong or weak signals, respectively. All protein bands were acquired with the iBright FL1500 imaging system (Thermo Fisher Scientific). All unprocessed, uncropped blots are shown in Suppl. Figures 1–5.

2.7 | Tandem mass tag (TMT) labelling of peptides followed by LC-MS/MS

Saline and cocaine total EV samples ($n = 3$ male mice per group) were solubilised with 8 M urea (Bio-Rad Laboratories, Hercules, CA, US) and processed as described elsewhere (Villen & Gygi, 2008). TMT labelling of purified peptides and the remaining proteomics procedures were performed as previously described (Erdjument-Bromage et al., 2018; Huang et al., 2017) with minor adjustments, as follows. TMT Label 126, 127N, 127C, 128N, 128C, 129N, 129C, 130N, 130C, and 131 (TMT10 plex Mass Tag Labeling Kit, Thermo Fisher Scientific) were added to each sample at a *w/w* label/peptide ratio of 12:1 and mixed briefly by vortexing. The mixture was incubated at room temperature for 1 h, quenched with 10 μ l 5% *w/v* hydroxylamine (Sigma-Aldrich), and then acidified with 10 μ l 10% *v/v* formic acid (Thermo Fisher Scientific). An aliquot from each reaction was desalted with Empore C18 High Performance Extraction Disks (3 M, St. Paul, MN, US). The eluted peptides were partially dried under vacuum and analyzed by LC-MS/MS with a Q Exactive High Field Orbitrap mass spectrometer (Thermo Fisher Scientific) to determine labelling efficiencies—which were found to be 97%–98%. To ensure equal amounts of labelled peptides, samples were mixed and analyzed in test runs by LC-MS/MS. The final sample mixture containing mixed TMT channels was prepared by readjusting the volume of each sample so that they contained equal amounts of labelled peptides (Suppl. Figure 6). The mixture was desalted by using a Sep-Pak tC18 1 cc Vac Cartridge (Waters Corporation, Milford, MA, US). Eluted peptides were analyzed in replicates by using LC with a Thermo Easy nLC 1000 system coupled online to a Q Exactive HF with a NanoFlex source (both systems from Thermo Fisher Scientific), as previously described (Huang et al., 2017).

2.8 | Transmission electron microscopy (TEM) imaging of mitochondria

Neuro-2a cells were cultured in a six-well dish and treated for 24 h either with 1 mM cocaine or with an equivalent volume of saline (control) in Opti-MEM, washed in PBS, fixed in EM fixative (0.1 M sodium cacodylate, 2.5% *w/v* glutaraldehyde, 2% *w/v* paraformaldehyde, pH 7.4, all reagents from Electron Microscopy Sciences, Hatfield, PA, US) and left at 4°C for at least 24 h. Cells were then treated with 1% *w/v* osmium tetroxide (Electron Microscopy Sciences) for 45 min and washed twice before being incubated with 1% *w/v* uranyl acetate (Electron Microscopy Sciences) overnight at 4°C. Cells were again washed twice and incubated with increasing concentrations of ethanol for 15 min each before being infiltrated with increasing concentration

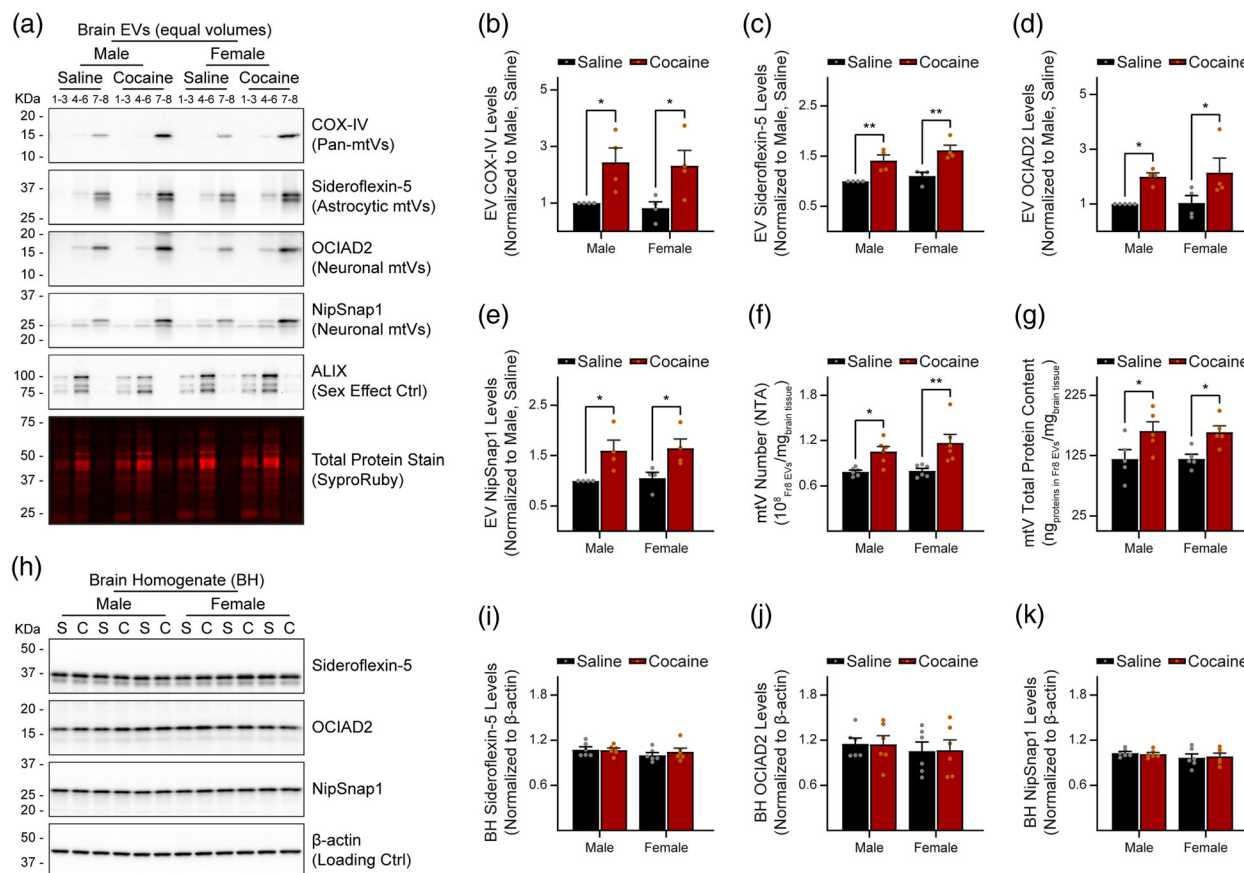


FIGURE 3 Mitovesicle extracellular levels are enhanced in the brain of cocaine-intoxicated mice. (a) Representative Western blot analyses of equal volumes (5 μ l) of brain extracellular vesicle (EV) lysates from either saline- or cocaine-treated male or female mice after high-resolution iodixanol step-gradient separation (Fractions 1–3, 4–6, and 7–8 combined). The isolation was performed on four samples at a time, one right hemisphere for each experimental group. EV fractions 1–3 were enriched in microvesicles, fractions 4–6 in exosomes, fractions 7–8 in mitovesicles (mtVs). SyproRuby total protein stain is shown as a control. KDa: kilodaltons. Uncropped, unprocessed blots are available in Suppl. Figure 4a. (b–e) Densitometric quantifications of the bands corresponding to the proteins COX-IV (b), Sideroflexin-5 (c), OCIAD2 (d), and NipSnap1 (e) in brain extracellular vesicle (EV) lysates analyzed by Western blot, as specified in (a). Quantifications were performed combining the signal from all the fractions, normalised to the weight of the brain tissue from which EVs were isolated. Graphs are plotted as a fold change over the saline-injected male within each isolation. Bars represent mean \pm SEM. $n = 4$ mice per group. Statistical test: two-way ANOVA (variables: treatment; sex) with Bonferroni's multiple comparisons test. * $P < 0.05$, ** $P < 0.01$. (f) Particle number quantification of mitovesicles isolated from the right hemisphere of either saline- or cocaine-treated male or female mice, as estimated by NTA. Fraction 8 (Fr8) mitovesicles alone were considered in this analysis given the higher mitovesicle purity of this sample when compared to fractions 7–8 combined. The number of Fr8 EVs (expressed as 100 million EVs) was normalised for each experimental group to the weight of the brain tissue from which EVs were isolated (expressed in mg). Bars represent mean \pm SEM. $n = 6$ mice per group. Statistical test: two-way ANOVA (variables: treatment; sex) with Bonferroni's multiple comparisons test. * $P < 0.05$, ** $P < 0.01$. (g) Quantification of mitovesicles isolated from the right hemisphere of either saline- or cocaine-treated male or female mice, as estimated by the BCA assay for total protein content. Fraction 8 (Fr8) EVs alone were considered in this analysis given the higher mitovesicle purity of this sample when compared to fractions 7–8 combined. The amount of proteins found in Fr8 EVs (expressed as ng) was normalised for each experimental group to the weight of the brain tissue from which EVs were isolated (expressed in mg). Bars represent mean \pm SEM. $n = 5$ mice per group. Statistical test: two-way ANOVA (variables: treatment; sex) with Bonferroni's multiple comparisons test. * $P < 0.05$. (h) Representative Western blot analyses of equal amounts (10 μ g protein, as estimated by BCA assay) of brain homogenates (BH) from either saline- or cocaine-treated male or female mice. 3 different mice per experimental group are shown. Homogenisation was performed for all samples at the same time. S: saline-treated mouse; C: cocaine-treated mouse. KDa: kilodaltons. Uncropped, unprocessed blots are available in Suppl. Figure 4b. (i–k) Densitometric quantifications of the bands corresponding to the proteins Sideroflexin-5 (i), OCIAD2 (j), and NipSnap1 (k) in brain homogenates (BH) analyzed by Western blot, as specified in (h). β -actin was used as the loading control. Graphs are plotted as a fold change over the first lane of the set (male, saline condition #1). Bars represent mean \pm SEM. $n = 6$ mice per group. Statistical test: two-way ANOVA (variables: treatment; sex) with Bonferroni's multiple comparisons test.

of Spurr resin (Electron Microscopy Sciences) for 1 h each. Finally, cells were left in 100% Spurr resin overnight. Excess Spurr resin was drained from the wells and a BEEM capsule (Electron Microscopy Sciences), which was filled with 100% Spurr resin, was inverted and placed over the cells. The plate with capsules was polymerised in an oven at 65°C overnight. Next day, the BEEM capsules were removed and sectioned using a Diatome diamond knife (Ted Pella Inc., Redding, CA, US) and a Reichert Ultracut S ultramicrotome (Leica, Wetzlar, Germany). 70-nm-thick sections were collected onto 75 mesh formvar and carbon-coated grids (Ted Pella Inc.). The grids were then incubated with 1% w/v uranyl acetate, washed, and finally incubated with lead

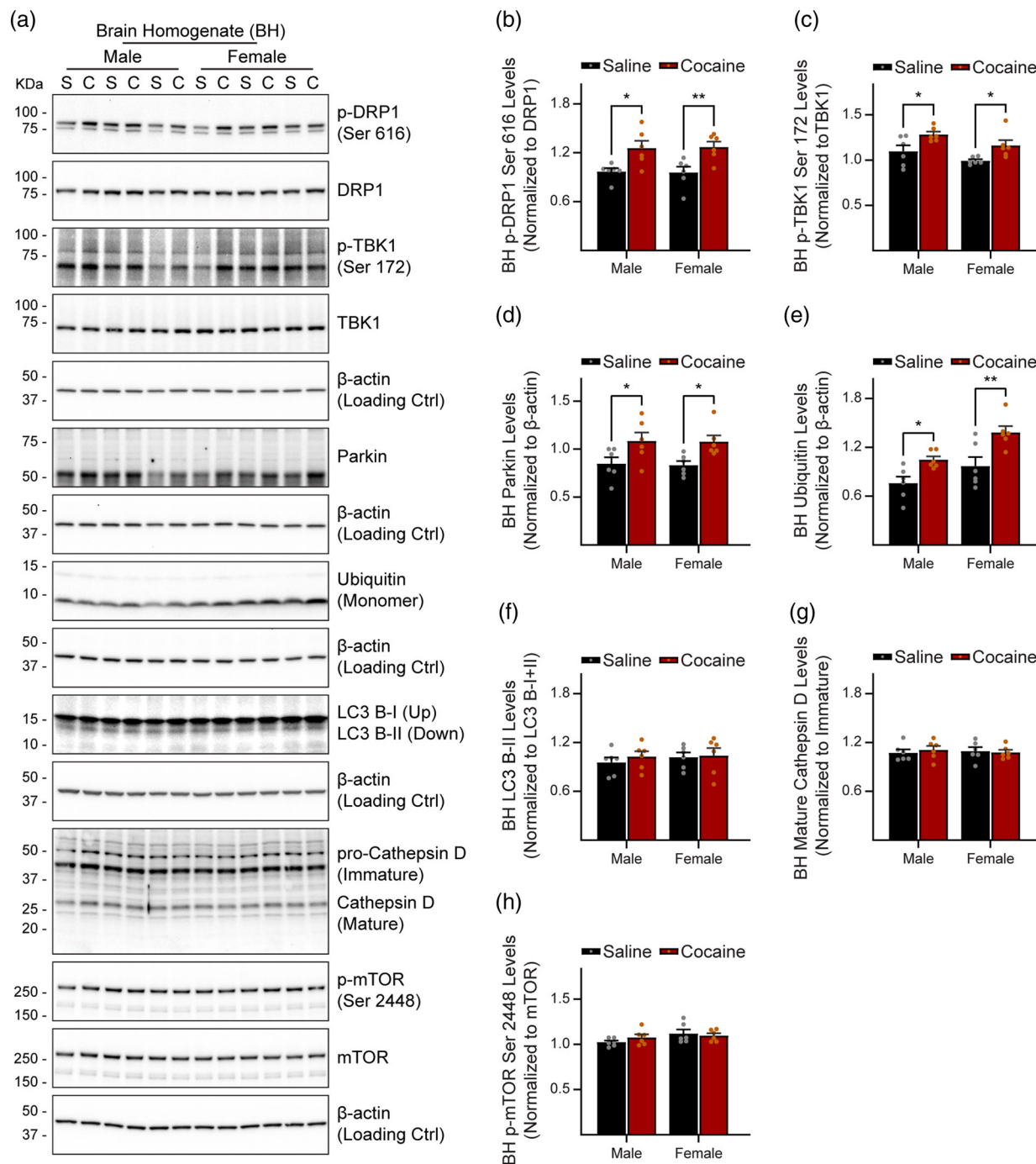


FIGURE 4 Cocaine alters the levels of proteins involved in the regulation of mitochondrial dynamics in the brain. (a) Representative Western blot analyses of equal amounts (5 μ g protein, as estimated by BCA assay) of brain homogenates (BH) from either saline- or cocaine-treated male or female mice. Three different mice per experimental group are shown. Homogenisation was performed for all samples at the same time. S: saline-treated mouse; C: cocaine-treated mouse. KDa: kilodaltons. Uncropped, unprocessed blots are available in Suppl. Figure 4. (b-i) Densitometric quantifications of the bands corresponding to the phospho-protein p-DRP1 (position 616) (b), the phospho-protein p-TBK1 (position 172) (c), and the proteins Parkin (d), Ubiquitin (e), LC3 B (f), Cathepsin D (g), as well as the phospho-protein p-mTOR (position 2448) (h) in brain homogenates (BH) analyzed by Western blot, as specified in (a). β -actin was used as the loading control, while phospho-proteins were normalised to the total, unphosphorylated counterparts. Graphs are plotted as a fold change over the first lane of the set (saline-injected male). Bars represent mean \pm SEM. $n = 6$ mice per group. Statistical test: two-way ANOVA (variables: treatment; sex) with Bonferroni's multiple comparisons test. * $P < 0.05$, ** $P < 0.01$

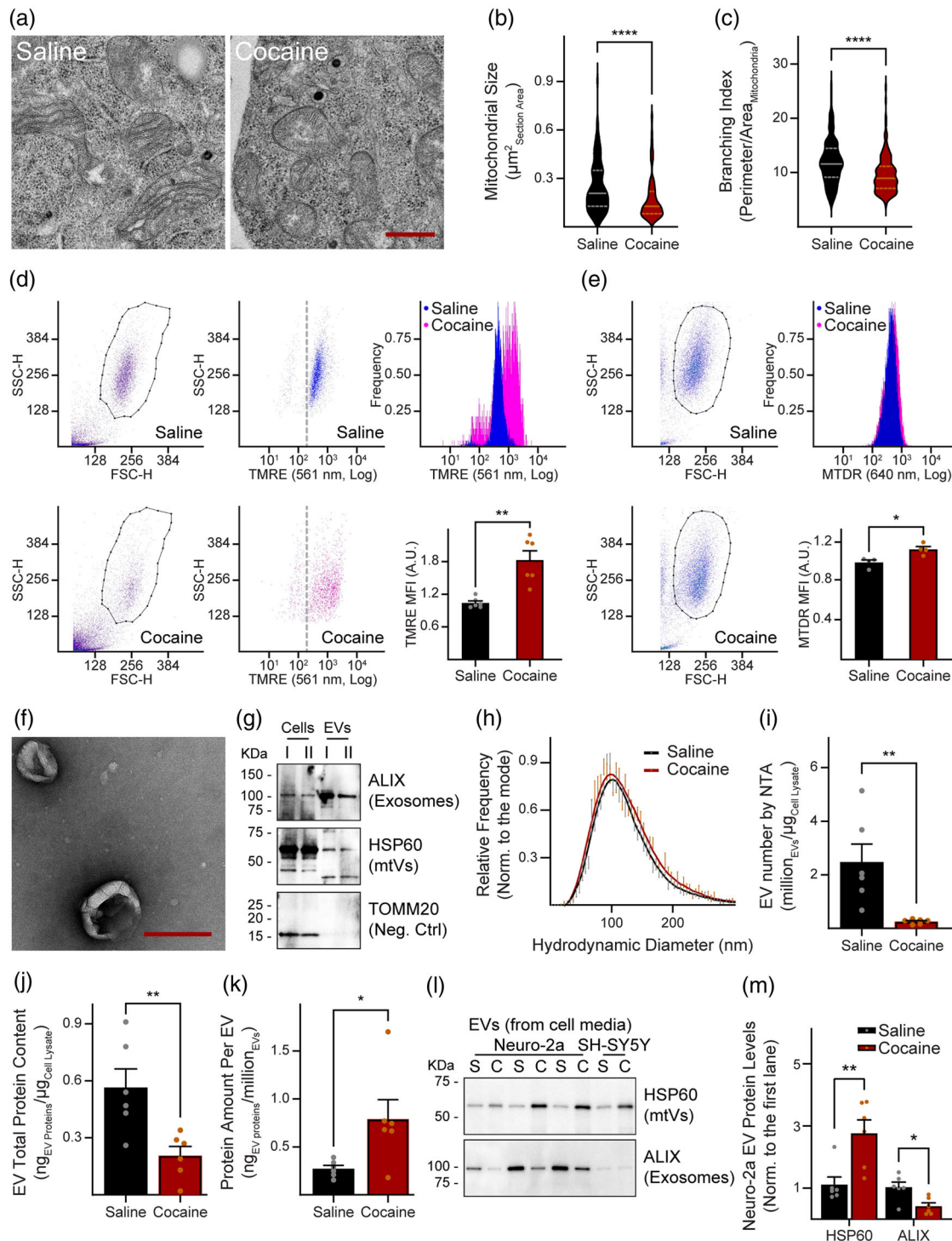


FIGURE 5 Cocaine effects on mitochondria, EVs, and mitovesicles of Neuro-2a cells in vitro. (a) Representative photomicrographs of fixed Neuro-2a cells treated or not with 1 mM cocaine for 24 h and imaged under transmission electron microscopy. Note the presence of mitochondria with altered *cristae* morphology in cocaine-treated cells. Scale bar: 500 nm. (b-c) Area distribution (b) and branching index (c) of Neuro-2a cell mitochondria treated or not with 1 mM cocaine for 24 h and imaged as in (a). Distributions are shown as violin plots (full line: median; dashed lines: 1st and 3rd quartiles). Number of mitochondria analyzed: 134 for the saline group and 161 for the cocaine group, respectively. Statistical test: Mann-Whitney *U* test. *****P* < 0.0001. (d-e) Flow cytometry analysis of Neuro-2a cells treated either with saline (upper rows) or with 1 mM cocaine (lower rows) for 24 h and stained either with TMRE (d) or MTDR (e). Both panels show the gating strategy (left columns), the representative fluorescence distribution of one experiment (right upper columns; the cell count on the y-axis was normalised to the mode of the distribution, while the x-axis is in a log₁₀ scale, indicated with 'Log') and the mean fluorescence intensity (MFI) per cell, expressed as arbitrary units (A.U., right lower columns). For TMRE staining, the gated population of cells and the relative TMRE intensity of one experiment are shown (with the x-axis in a log₁₀ scale, indicated with 'Log', middle columns). Autofluorescence controls (cells without dye) were performed for each experiment; dashed lines indicate the maxima recorded for these controls. SSC-H: side scatter—height. FSC-H: forward scatter—height. Bars represent mean ± SEM. *n* = either 6 (d) or 4 (e) independent experiments. Statistical test: Student's *t*-test. **P* < 0.05, ***P* < 0.01. (f) Representative TEM

(Continues)

FIGURE 5 (Continued)

photomicrographs (negative stain) of fixed EVs secreted by Neuro-2a cells, displaying EV typical cup-shaped morphology and the absence of contaminating membranes and cell debris. Scale bar: 200 nm. (g) Representative Western blot analyses of equal amounts (1 μ g proteins, as estimated by BCA assay) of Neuro-2a cell lysates ('Cells' lanes) and Neuro-2a EV lysates ('EVs' lanes). 2 independent experiments are shown as Latin numbers I and II. kDa: kilodaltons; mtVs: mitovesicles. Uncropped, unprocessed blots are available in Suppl. Figure 5a. (h) Hydrodynamic diameter distribution of EVs secreted by Neuro-2a cells treated or not with 1 mM cocaine for 24 h, as assessed by NTA. The distributions were normalised to the mode, while the bell curves were obtained using a nine-point moving average. $n = 7$ independent EV isolations per experimental group. (i) Particle number quantification of EVs secreted by Neuro-2a cells treated or not with 1 mM cocaine for 24 h, as estimated by NTA. The number of EVs (expressed as million EVs) was normalised for each isolation to the total amount of cells from which EVs were recovered (expressed as μ g of cell lysate). Bars represent mean \pm SEM. $n = 6$ independent EV isolations per experimental group. Statistical test: Student's *t*-test. $**P < 0.01$. (j) Quantification of EVs secreted by Neuro-2a cells treated or not with 1 mM cocaine for 24 h, as estimated by the BCA assay for total protein content. The amount of proteins found in EVs (expressed as ng) was normalised for each isolation to the total amount of cells from which EVs were recovered (expressed as μ g of cell lysate). Bars represent mean \pm SEM. $n = 6$ independent EV isolations per experimental group. Statistical test: Student's *t*-test. $**P < 0.01$. (k) Quantification of the protein content per single Neuro-2a EV upon treatment or not with 1 mM cocaine for 24 h, calculated as the ratio between the amount of protein (as estimated by the BCA assay for total protein content and expressed as ng) and the number of EVs (as estimated by NTA and expressed as million EVs) for each isolation. Bars represent mean \pm SEM. $n = 6$ independent EV isolations per experimental group. Statistical test: Student's *t*-test. $*P < 0.05$. (l) Representative Western blot analyses of equal volumes (5 μ l) of EVs isolated from the cell culture medium of either Neuro-2a or SH-SY5Y cells treated or not with 1 mM cocaine for 24 h. Each lane corresponds to an independent EV isolation. S: EVs from saline-treated cells; C: EVs from cocaine-treated cells; kDa: kilodaltons; mtVs: mitovesicles. Uncropped, unprocessed blots are available in Suppl. Figure 5b. (m) Densitometric quantifications of the bands corresponding to the proteins HSP60 and ALIX in EV lysates analyzed by Western blot, as specified in (l). Graphs are plotted as a fold change over the signal found in the first lane (EVs from saline-treated cells). Bars represent mean \pm SEM. $n = 6$ independent EV isolations per experimental group. Statistical test: Student's *t*-test. $*P < 0.05$, $**P < 0.01$.

citrate (Electron Microscopy Sciences) before being washed once more. The cells were imaged on a Talos L120C transmission electron microscope (Thermo Fisher Scientific) operating at 120 kV and the images collected with a Ceta camera (Thermo Fisher Scientific).

2.9 | Flow cytometric measurement of mitochondrial mass and membrane potential

Neuro-2a cells were cultured in 35 mm tissue culture dishes at a density of 4×10^5 cells and treated for 24 h either with 1 mM cocaine or with an equivalent volume of saline (control) in Opti-MEM. Subsequently, cells were trypsinised and collected in DMEM at the concentration of 10^6 cells/ml. These suspensions were incubated in a water bath at 37°C for 30 min with MitoTracker Deep Red FM (hereafter MTDR, Thermo Fisher Scientific) at a final concentration of 200 nM, or with tetramethylrhodamine ethyl ester (hereafter TMRE, Thermo Fisher Scientific) at a final concentration of 400 nM, following manufacturer's instructions. Flow cytometry analyses were carried out on a BigFoot cell sorter (Thermo Fischer Scientific) using the standard 100 μ m nozzle tip with a pressure of 30 psi (pound-force per square inch). MTDR was acquired using a 640 nm laser with a 670/30 nm bandpass filter, while TMRE was excited with a 561 nm laser and acquired with a 575/15 nm bandpass filter, both measured on a linear scale. 10,000 events (cells) were acquired for each experimental condition and for each replicate. Data were analyzed using the built-in Sasquatch software (Thermo Fisher Scientific) in order to obtain the mean fluorescence intensity (MFI) for each mitochondrial dye.

2.10 | Other EV analyses

Murine brain mitovesicles and EVs from conditioned cell media were analyzed by cryo-EM, TEM, NTA, and ATP determination assays as previously described in detail (D'Acunzo et al., 2021; D'Acunzo et al., 2022). Per MISEV2018 guidelines, the level of EVs, including mitovesicles, should be determined using at least two unbiased, independent methods (Thery et al., 2018). Therefore, to estimate the number of secreted mitovesicles and of total EVs from conditioned media we performed both NTA (Figures 3f and 5i) and the BCA assay for total protein content (Figures 3g and 5j) following manufacturer's instructions, as previously described (D'Acunzo et al., 2021; Gauthier et al., 2017; Peng et al., 2019). For in vivo experiments, both NTA and BCA data were normalised to the weight of the brain tissue from which mitovesicles were isolated. For in vitro experiments, NTA and BCA data were normalised to the total amount of proteins found in cell lysates, an indirect measure of the number of producing cells.

3 | RESULTS

3.1 | Cocaine stimulates the production of enlarged mitovesicles

To study the impact of chronic cocaine exposure on mitovesicle biology, we injected intraperitoneally male and female C57BL/6J mice, starting at 2.5 months of age, once-daily for 12 days with either saline or cocaine (10 mg/kg body weight). EVs were

isolated from the right hemibrains of these mice and fractionated through a high-resolution density gradient to separate EV subpopulations, as previously described by us (Barreto et al., 2022; D'Acunzo et al., 2021, 2022) and others (Jeppesen et al., 2019).

As assessed by Western blot analysis (Figure 1a), with our fractionation system microvesicle proteins, such as Annexin A2, were enriched in low-density fractions (with the highest signal in fractions 1–3) while exosome proteins, such as ALIX, were mainly found in the intermediate-density fractions 4–6 (with a minor presence in fractions 3 and 7), consistent with previous reports (Barreto et al., 2022; Jeppesen et al., 2019; D'Acunzo et al., 2021, 2022). The brain EVs in the highest density fractions, particularly in Fr8, were largely negative for microvesicle and exosome proteins and contained mitovesicles, as assessed by the levels of mitochondrial proteins such as PDH α , found in the mitovesicle matrix (MMx), COX-IV, found in the inner mitovesicle membrane (IMM), and VDAC, found in the outer mitovesicle membrane (OMM). These mitovesicle proteins were not only enriched in Fr8 EVs as opposed to other EV fractions, but also when Fr8 EVs were compared to the respective left hemibrain homogenates (Figure 1a, BH lane) in which the signal derives mostly from intracellular mitochondria. Small EVs, including mitovesicles, have a higher surface/volume ratio compared to the organelles from which they originate, implying a higher membranous/luminal protein ratio in mitovesicles than in mitochondria. In agreement with that, the enrichment of mitovesicle proteins in Fr8 brain EVs as compared with brain homogenates was more prominent for IMM and OMM proteins than for MMx proteins. As a negative control, we also confirmed the absence in our brain EV preparations of proteins from unrelated intracellular compartments—an indication of EV purity. Among others, we checked for the Golgi apparatus (assessed by the Golgi protein GM130), the endoplasmic reticulum (assessed by SEC61B, a subunit of the translocon complex), and potential intracellular mitovesicle-related contaminants such as MDVs and whole mitochondria, assessed by the mitochondrial proteins MFN2, TSPO, and TOMM20 (Figure 1a). The latter are abundantly found within a cell (and, accordingly, in brain homogenates), but are not secreted into the extracellular space via mitovesicles, as these EVs carry only a restricted, mostly catabolic set of mitochondrial proteins (D'Acunzo et al., 2021).

The isolation of mitovesicles in Fr8 was further corroborated by cryo-EM (Figure 1b). Under cryo-EM, mitovesicles are easily detectable since they are uniquely characterised by a very dense MMx, a concentric double membrane (IMM and OMM, respectively), a narrow (<6 nm) intermembrane space (IS), and the absence of *cristae* (D'Acunzo et al., 2021). Consistent with the Western blot data, we found EVs with all these features in Fr8 but not in the other fractions.

Measurement of the diameter of the brain mitovesicles observed by cryo-EM revealed that mitovesicles isolated from the brain of mice treated with cocaine were bigger than mitovesicles isolated from saline-treated mice (Figure 1b,c). This difference in size was confirmed by NTA (Figure 1d,e), suggesting that, once incorporated into mitochondria, cocaine stimulates the production of abnormally large vesicles.

3.2 | Brain mitovesicle protein composition and ATP production capacity are altered by cocaine in a sex-specific fashion

Comparison of the proteome of the EVs released into the brain extracellular space using LC-MS/MS revealed differences in multiple proteins between cocaine-injected and saline-injected male mice (Figure 2a and Suppl. Table 1). Several proteins in male brain EVs whose levels were altered after chronic cocaine administration *in vivo* were involved in neurotransmission, including neurotransmitter-related metabolic enzymes (GAD2), synaptic proteins (SV2B), axon morphology regulators (FLRT3, GNG7, CPNE1, EMB, PPP3R1), and ion channels (ATP1A2, SCN2B, CACNG3, SLC9A3R1, SLC1A2, Suppl. Table 1). This finding is consistent with a model in which brain EVs contribute to complex synaptic alterations in recipient cells upon long-term cocaine exposure. Moreover, the presence of higher levels of the protein FLRT3 in brain EVs of cocaine-treated male mice (Suppl. Table 1) mirrors the change found in human hippocampi of males with cocaine use disorder (Mash et al., 2007), suggesting that brain EVs can potentially be valuable diagnostic tools to predict perturbations found within a cell. The most numerically prominent differences found in our LC-MS/MS analysis were, however, mitovesicle-related (Figure 2a). Eighteen mitovesicle proteins were at lower levels in brain EVs of cocaine-treated male mice when compared to saline-treated controls: three out of 45 (~7%) subunits of the ETC complex I, six out of 15 (40%) subunits of the ETC complex V (also known as ATP synthase), two OMM pores for small hydrophilic molecules, including pyruvate, ATP, and ADP (VDAC and VDAC2), two IMM antiport carriers for respiratory substrates (SLC25A11 and SLC25A12), one IMM amino acid transporter (SFXN3), one MMx enzyme involved in fatty acid metabolism (ACSL6), one MMx enzyme of the Krebs' cycle (DLST), and two multifunctional proteins (PHB and CIQBP). No differences in the levels of ETC complex II, complex III, or complex IV subunits were found.

Western blot analyses were used to validate the differences identified by LC-MS/MS and to investigate whether there were sex-differences in the response to cocaine (Figure 2b–e). Most of the mitovesicle proteins affected by cocaine treatment were involved in bioenergetic pathways, either directly (ETC complex subunits and other metabolic enzymes) or indirectly (metabolite/ion channels, uniporters, and antiporters). Thus, we focused our attention on the levels of proteins involved in ATP production (ETC complex subunits) and indirect modulators (VDAC), as assessed by Western blot analyses of equal amounts (0.5 μ g total protein) of mitovesicle lysates. Given its importance in the regulation of dopamine levels, we also explored the possibility that MAO-A (a neuronal mitochondrial protein involved in the degradation of monoaminergic neurotransmitters including norepinephrine,

serotonin, and dopamine; Cho et al., 2021), was differentially found in mitovesicles isolated from the brain of cocaine- or saline-treated mice (Figure 2b–e). Western blot data confirmed that cocaine impaired the loading into mitovesicles in the brain of males of VDAC, MAO-A, several ETC complex V subunits (ATP5A1, ATP5B) and specific ETC complex I subunits (NDUFA5), but not others (NDUFB8). The ETC complex II and complex IV tested (SDHB, COX-IV) and the IMM/IS protein OPA1 were unchanged, consistent with the LC-MS/MS data (Figure 2a–e). In mitovesicles isolated from female brains, the only differentially present protein was MAO-A, indicating that cocaine causes both sex-dependent (VDAC, ATP5A1, ATP5B, NDUFA5) and -independent (MAO-A) alterations in mitovesicle composition.

We previously demonstrated that mitovesicles can produce ATP *in vitro* through the same ETC complexes altered by cocaine (D'Acunzo et al., 2021), including complex V. Accordingly, we hypothesised that mitovesicles isolated from the brain of male, but not female mice chronically exposed to cocaine would be specifically impaired in their ability to produce energy when compared to saline controls. The measurement of the amount of ATP produced *in vitro* after incubation of mitovesicles for 10 min at 37°C with oxidative phosphorylation substrates and cofactors (malate, pyruvate, ADP, Mg²⁺) confirmed the sex difference in energy production by mitovesicles (Figure 2f). We then checked whether mitovesicle cargo alterations were due to sex-dependent downregulation of the cognate intracellular proteins. No differences in the expression levels of these proteins were identified in the respective brain homogenates (Figure 2g–p), suggesting that mitovesicle composition abnormalities induced by cocaine are EV-specific and do not passively mirror similar changes in the cells of origin.

3.3 | Cocaine causes accumulation of mitovesicles in the brain extracellular space

To explore the possibility that cocaine perturbs the levels of mitovesicles released into the brain extracellular space upon chronic exposure (Figure 3a–g), equal volumes of brain EV lysates isolated from either saline- or cocaine-treated male or female mice were loaded on a polyacrylamide gel and checked for mitovesicle markers by Western blot analysis (Figure 3a–e). When equal EV volumes (μl lysates) instead of equal EV amounts (μg total protein) are loaded, the Western blotting signal of a desired protein is dependent on both the quantity of the protein per EV and on the amount of EVs positive for the protein analyzed. However, when the quantity of a specific protein per EV is not altered (as is COX-IV in our experimental conditions, see Figure 2b), the signal is solely proportional to the levels of EVs bearing that specific protein. Thus, we investigated the levels of four mitovesicle proteins (COX-IV, Sideroflexin-5, NipSnap1, OCIAD2) which showed that: (I) their mitovesicle cargo loading was invariant between the groups, as assessed by our LC-MS/MS-analysis (Suppl. Table 1) or by Western blotting data loading equal amounts of mitovesicles (Figure 2b); and (II) their intracellular expression level was unaltered, as demonstrated by Western blot analysis of brain homogenates (Figures 2p and 3h–k). COX-IV is ubiquitously expressed and as such can be considered a pan-mitovesicle marker. Sideroflexin-5 expression is astrocyte-specific, while NipSnap1 and OCIAD2 are expressed exclusively in neurones (Fecher et al., 2019). Accordingly, these proteins can be used to evaluate the relative amount in the extracellular space of the whole mitovesicle population, of astrocytic mitovesicles, and of neuronal mitovesicles, respectively. As a control of the sex-specific effect of cocaine on EVs, we assessed ALIX (whose levels are proportional to the number of exosomes, as previously shown; Barreto et al., 2022). While ALIX protein levels were lower in males chronically exposed to cocaine and unaltered in females, as previously shown (Barreto et al., 2022), the levels of all mitovesicle markers were higher in cocaine-treated mice of both sexes when compared to controls (Figure 3a–e). The largest fold change was detected for COX-IV (roughly +150%, Figure 3b) while Sideroflexin-5 was roughly +50% (Figure 3c) and OCIAD2 roughly +80% (Figure 3d), consistent with COX-IV presence in both Sideroflexin-5-positive and OCIAD2-positive mitovesicles. The higher number of mitovesicles in the brain extracellular space of both male and female mice upon chronic cocaine exposure was further confirmed by NTA (Figure 3f) and total protein quantification (Figure 3g).

Altogether, these data show that neuronal-derived and astrocytic-derived mitovesicles are found at higher levels in the brain extracellular space of both male and female mice when treated daily with cocaine for 12 days.

3.4 | After repetitive cocaine exposure, murine brains display molecular signs of mitochondrial abnormalities

We have previously shown both *in vitro* and *in vivo* that mitovesicle secretion is enhanced when damaged mitochondria accumulate (D'Acunzo et al., 2021), likely a homeostatic mechanism to eliminate detrimental mitochondrial material from the cell and mitigate the intracellular production of reactive oxygen species (ROS). Cocaine is a well-established inducer of mitochondrial impairment in all brain areas, especially after prolonged exposure (as reviewed in Thornton et al., 2021), and cocaine validated biological activities include the stimulation of mitochondrial fission via phosphorylation of DRP1 and a block of mitophagy (Funakoshi et al., 2019; Thangaraj et al., 2020; Wen et al., 2022), an intracellular quality control pro-survival mechanism that reduces the mass of damaged mitochondria (D'Acunzo et al., 2019; Di Rita, D'Acunzo, et al., 2018; Di Rita, Peschiaroli, et al., 2018; Di Rita et al., 2021).

With this in mind, we hypothesised that chronic cocaine exposure would stimulate alterations of proteins and pathways involved in mitochondrial homeostasis, leading to the secretion of higher levels of mitovesicles into the brain extracellular space of both male and female mice (Figure 3a–g). Accordingly, we analyzed the levels of a master regulator of mitochondrial fission, DRP1, as well as its activation status (p-DRP1, serine 616), in the brain homogenates of mice chronically treated with cocaine. When phosphorylated at position 616, DRP1 is activated, leading to higher mitochondrial fission and potentially neuronal death, as has been extensively demonstrated (Chandra et al., 2017; Gao et al., 2022; D. I. Kim et al., 2016; Luo et al., 2017; Roe & Qi, 2018). We found that, upon cocaine administration, DRP1 protein levels did not change, while its active phosphorylated form increased in both male and female mice (Figure 4a–c).

In addition, we explored in both sexes the levels of key mitophagy proteins upon chronic cocaine exposure. Analysis of the active form of the mitophagy master regulator TBK1 (p-TBK1, serine 172; Heo et al., 2015; Heo et al., 2018; Richter et al., 2016), the effector protein Parkin, and the mitophagy-recruiting protein Ubiquitin, which decorates the surface of damaged mitochondria targeted for degradation (Richter et al., 2016), revealed that these proteins and post-translational modifications were upregulated in cocaine-treated brains when compared to saline-treated controls (Figure 4a and d–f). However, consistent with previous in vitro reports (Thangaraj et al., 2020), markers of autophagy progression (lipidation and activation of the autophagosome protein LC3 B, phosphorylation of the autophagy master regulator mTOR, serine 2448; Tomaipitina et al., 2021) and of lysosomal activity (cleavage of the immature lysosomal proteolytic enzyme cathepsin D into its mature form; Zaidi et al., 2008) did not differ between the groups (Figure 4a and g–i), suggesting no stimulation of autophagy.

Thus, analysis of the brain of cocaine-intoxicated male and female mice revealed the presence of sex-independent changes in proteins that are crucial for maintenance of mitochondrial homeostasis. These data are consistent with the presence of cocaine-induced mitochondrial alterations under our experimental conditions and are in full agreement with what was previously published by other independent groups (Funakoshi et al., 2019; Thangaraj et al., 2020; Thornton et al., 2021; Wen et al., 2022).

3.5 | EVs from Neuro-2a cells treated with cocaine in vitro mirror the EV and mitovesicle alterations found in the brain extracellular space of mice in vivo

For a direct study of the interrelationship between cocaine-induced mitochondria alterations and mitovesicle secretion, undifferentiated murine neuroblastoma Neuro-2a cells were incubated with cocaine or saline as controls for 24 h and the resulting effects on mitochondria (Figure 5a–e) and EVs (Figure 5f–m) analyzed. Unlike the human cognate SH-SY5Y cells (Cheung et al., 2009), untransfected Neuro-2a cells do not express the dopamine transporter *Dat* (L. Zhang et al., 1998) and do not show dopamine uptake in vitro (L. Zhang et al., 1998), and therefore were used here to study cocaine-induced but dopamine-dispensable cell alterations, including mitochondrial (Funakoshi et al., 2019) and endosomal/exosomal (Barreto et al., 2022) perturbations. Moreover, as Neuro-2a cells were originally isolated from male mice and oestrogens were never added to cell culture media in our experiments, these cells are potentially ideal to reproduce changes induced by cocaine in EVs in the brain extracellular space of male mice, including a reduction in exosome secretion (Barreto et al., 2022).

Cocaine treatment did not induce cell death: the percentage of dead cells, as assessed by Trypan Blue staining in 6 independent experiments, was 5.94 ± 1.79 versus $5.63 \pm 1.89\%$ (mean \pm SEM; $P = 0.9150$) for saline- and cocaine-treated cells, respectively. However, consistent with what previously reported (Funakoshi et al., 2019), cocaine-treated cells displayed signs of mitochondrial alterations (Figure 5a–e). TEM investigation revealed that mitochondria of cocaine-treated cells were more numerous (Figure 5a), showed with a higher frequency the presence of disrupted *cristae* (55% of cocaine-treated cell mitochondria did not display normal *cristae* morphology, Figure 5a), were smaller (Figure 5a,b), and less branched (Figure 5c). Furthermore, the mitochondrial potential across the MIM ($\Delta\Psi_m$) was higher in cells treated with cocaine when compared to controls, as assessed in living cells by the MFI emitted by TMRE, a $\Delta\Psi_m$ -dependent fluorophore (Figure 5d). Lastly, as assessed by the MFI emitted by MTDR, the total mass of mitochondria per cell was higher in cocaine- versus saline-treated cells (Figure 5e), an indication of a reduced mitochondrial turnover. Altogether, these data demonstrate that cocaine elicited a complex network of mitochondrial alterations that led to the intracellular accumulation (Figure 5e) of abnormal (Figure 5a–d) mitochondria.

We next examined the impact of cocaine on small EVs released by Neuro-2a cells (Figure 5f–m). Owing to the paucity of the sample, small EVs from conditioned media were not fractionated using the density gradient separation method described above for brain EVs. Therefore, our analyses focused on the total pool of small EVs released by Neuro-2a cells (Figure 5f). As assessed by Western blot analyses, these EVs were enriched in exosomes (see the enrichment of ALIX in EVs as compared to cell lysate, Figure 5g), and contained mitovesicles (under physiological conditions, ~1% of the total EV population, D'Acunzo et al., 2021; 'HSP60' line in Figure 5g). Prolonged (24 h) cocaine exposure did not cause a global change in the size of total EVs, as assessed by NTA in 6 independent isolations (Figure 5h): the median hydrodynamic diameters of EVs from saline- and cocaine-treated cells were 111.4 ± 3.09 versus 111.7 ± 3.26 nm, respectively (mean \pm SEM, $P = 0.8664$, full distribution profile shown in Figure 5h), consistent with TEM data (Figure 5f). However, the conditioned media of Neuro-2a cells exposed to cocaine contained a reduced number of EVs when compared to controls, as assessed by NTA (Figure 5i) and total EV protein quantification (Figure 5j),

suggesting a cocaine-mediated reduction in the release of EVs. Given that Neuro-2a cells were never exposed to female sex hormones in our experiments, we posited that this effect of cocaine was mainly due to a block in the secretion of exosomes, as we previously reported in the brain of male mice chronically exposed to cocaine (Barreto et al., 2022) and further confirmed in this study (Figure 3a, line 'ALIX').

According to our *in vivo* data (Figure 3a–g and Barreto et al., 2022) cocaine reduced secretion of exosomes and stimulated higher secretion of mitovesicles. To demonstrate that this biological activity on EV release observed *in vivo* occurred also *in vitro*, we quantified the average amount of proteins per single EV, calculated as a ratio of protein amount to EV number, as estimated by BCA and NTA, respectively (Figure 5k). We found about three-fold higher average amount in EVs secreted by cocaine-treated cells (Figure 5k). As exosomes are characterised by a lower protein amount per single EV when compared to mitovesicles (D'Acunzo et al., 2021), data shown in Figure 5k suggest that more mitovesicles and less exosomes are released in the presence of cocaine as compared to saline controls.

In order to confirm this speculation, equal volumes of EVs produced by either saline- or cocaine-treated cells were loaded on a polyacrylamide gel and analyzed by Western blotting (Figure 5l,m), as discussed above for EVs isolated from the brain extracellular space *in vivo* (Figure 3a). We found higher levels of the mitovesicle marker HSP60 (around 200% higher signal, an amplitude consistent with our brain Western blot data when a pan-mitovesicle marker was analyzed, Figures 5l,m and 3a,b) and lower levels of the exosome marker ALIX (Figure 5l,m) in EVs from the cultured media of cocaine-treated cells as compared to saline controls. Similar results were obtained for SH-SY5Y cells (Figure 5l, last two lanes), revealing that the mitovesicle response elicited by cocaine occurs also in human cells.

4 | DISCUSSION

Our in-depth analysis of the effect of repeated cocaine treatment (once daily for 12 days) on brain mitovesicles revealed higher mitovesicle levels in the brain extracellular space of treated mice in both males and females, for both neuronal and astrocytic mitovesicles, and in several brain areas, given that mitovesicles were isolated from whole hemibrains (Figure 3a–e). Neuro-2a and SH-SY5Y cells treated with cocaine displayed similar results (Figure 5l,m). This is in agreement with the previously reported observation that cocaine can be incorporated into mitochondria of multiple cell types, as shown for cardiomyocytes (Yuan & Acosta, 2000), hepatocytes (Cunha-Oliveira et al., 2013a), and endothelial cells (He et al., 2000), where it induces mitochondrial dysfunction regardless of the presence of dopamine or the transporter DAT.

Higher levels of mitovesicles in the brain extracellular space can be either a result of a higher mitovesicle generation and/or secretion by producing cells, reduced mitovesicle uptake by recipient cells, or reduced clearance from the brain into the circulation. As the levels of cocaine within mitochondria increase with dosage frequency (Funakoshi et al., 2019), we posited that the pathway affected was the mitovesicle biogenesis, although we cannot exclude stimulating effects of cocaine on the exocytosis of pre-formed mitovesicles. Our *in vitro* data (Figure 5l,m) supported this speculation. Furthermore, brain mitovesicles of cocaine-treated mice were larger than controls (Figure 1), indicating interference of cocaine at the stage of mitovesicle production rather than secretion. Mitovesicles with a greater volume contain more material than smaller mitovesicles. Accordingly, the secretion of bigger mitovesicles (Figure 1) may work in synergy with the secretion of more mitovesicles (Figure 3) to eliminate a greater quantity of mitochondrial constituents when compared to the same number of smaller mitovesicles in order to attempt restoring normal mitochondrial physiology.

This hypothesis assumes compromised mitochondrial homeostasis after repetitive cocaine exposure, a cocaine-induced effect that was previously shown by several research groups (Funakoshi et al., 2019; Thangaraj et al., 2020; Wen et al., 2022; reviewed in Thornton et al., 2021), and found in the *in vitro* (Figure 5) and *in vivo* (Figure 4) experiments described here. In particular, mitochondria hyperpolarisation in cocaine-treated cells (Figure 5d) indicated an accumulation of H⁺ protons in the IMS, suggesting a downstream block of oxidative phosphorylation (as previously reported; Cunha-Oliveira et al., 2013a, 2013b; Yuan & Acosta, 2000) at the level of the ETC Complex V, where, under physiological conditions, the H⁺ gradient is dissipated to generate ATP. A dysfunction in the ETC Complex V was found in mitovesicles isolated from the brain of male mice chronically intoxicated with cocaine (Figure 2a,d,f), reinforcing the concept that brain EVs are potential predictors of brain cell perturbations. $\Delta\Psi_m$ is a master regulator of mitochondrial homeostasis and changes in $\Delta\Psi_m$ greatly affect mitochondria functionality. For instance, a decrease in $\Delta\Psi_m$ is necessary to induce mitophagy, regardless of the accumulation of ROS or other kinds of mitochondrial damage (Narendra et al., 2008; Narendra et al., 2010). If mitochondria are not depolarised, mitophagy is not induced, as PINK1 does not accumulate on the MOM and Parkin is not recruited onto the mitochondrial surface (Narendra et al., 2008; Narendra et al., 2010). Furthermore, the amount of H₂O₂ generated within mitochondria depends on $\Delta\Psi_m$ levels, and even subtle increases in $\Delta\Psi_m$ cause a sharp increment in mitochondrial H₂O₂ (Korshunov et al., 1997). Consequently, the higher $\Delta\Psi_m$ induced by cocaine (Figure 5d) may be the primary cause of several cocaine-related mitochondria effects, including (I) an enlarged mitochondrial mass (Figure 5e), a likely consequence of the lower mitochondria removal rate due to the inability to trigger mitophagy (not induced without a reduction of $\Delta\Psi_m$); (II) higher generation of mitochondrial ROS, including H₂O₂, an effect of cocaine that was

previously described (reviewed in Thornton et al., 2021); (III) lower ATP production, as described (Cunha-Oliveira et al., 2013a, 2013b; Yuan & Acosta, 2000), owing to an impairment in the ETC Complex V activity; and ultimately (IV) higher mitovesicle production, owing to a larger mass of mitochondria from which mitovesicle originate, and impaired mitovesicle cargo loading, likely owing to functional and morphological deficits (Figure 5a–e). In vivo, we found that the levels of regulators of mitochondrial homeostasis, such as DRP1, TBK1, and Parkin, in mice chronically exposed to cocaine were altered in a sex-independent fashion, while the levels of autophagy/lysosomal markers LC3 B-II, cathepsin D, and p-mTOR were unchanged (Figure 4), consistent with stimulation of mitophagy inducers, but not of autophagy/mitophagy progression. These data are consistent with our in vitro data and with previous reports of cocaine-intoxicated primary cells, showing upregulation of several upstream mitophagy proteins, including Parkin, and a parallel block of downstream autophagy-lysosomal pathways, effectively blocking mitophagy flux and leading to traffic jam (Thangaraj et al., 2020). Altogether, our data suggest that autophagy/mitophagy impairment (and consequent accumulation of mitochondrial mass), in concert with higher $\Delta\Psi_m$, may be the driver of the enhanced mitovesicle production and secretion, and is in agreement with a large body of evidence linking the loading and secretion of mitochondrial material via EVs with a block in intracellular mitochondrial quality control systems, including mitophagy, as a causative event (Beatriz et al., 2022; Crewe et al., 2021; Phinney et al., 2015; Picca et al., 2020; Rosina et al., 2022).

The most studied molecular target of cocaine, the dopamine transporter DAT, is not expressed by Neuro-2a cells (L. Zhang et al., 1998). This suggests that DAT is not required in order to elicit cocaine-induced mitochondria and mitovesicle changes. In vivo, *Dat* is expressed at relevant levels exclusively by dopaminergic neurones (Ciliax et al., 1999; Turiault et al., 2007), which are found mainly in the mesencephalon in the substantia nigra pars compacta and in the ventral tegmental area (Ciliax et al., 1999; Turiault et al., 2007). DAT is not found in astrocytes and in pyramidal neurones of the forebrain (Block et al., 2015), with the exception of the relatively scarce dopaminergic neurones found in the olfactory bulbs (Cave & Baker, 2009). Accordingly, it is conceivable that DAT-dependent cellular effects of cocaine are restricted to a numerically minor subset of neurones located in the midbrain and to the areas where they establish synapses, mostly the nucleus accumbens and other zones of the striatum (Ciliax et al., 1999). The evidence that the effects of chronic cocaine exposure were found in mitovesicles isolated from whole forebrains (Figure 3), including astrocytic mitovesicles (Figure 3a–c), and in mitochondria of total brain homogenates (Figure 4), suggests that cocaine affected mitochondria/mitovesicle homeostasis of a large proportion of cells in the forebrain and that the mechanism responsible for these alterations may be at least in part DAT- and dopamine-independent. This conclusion is supported by (I) our in vitro data using a cell line that does not express *Dat* (Figure 5), (II) the previously reported global reduction in brain metabolism in all forebrain regions (and not just the dopaminergic circuitry) of men with cocaine use disorder (London et al., 1990), as well as (III) the ATP production impairment induced by cocaine on cell-free isolated mitochondria in vitro (Cunha-Oliveira et al., 2013a, 2013b; Yuan & Acosta, 2000), demonstrating that cocaine triggers effects directly on mitochondria in a dopamine-dispensable fashion. Moreover, the brain of *Dat* knock-out (*Dat*-KO) mice treated with cocaine showed reduced metabolism and ATP production capacity when compared to the brain of saline controls (Thanos et al., 2008), mirroring data obtained in humans (London et al., 1990). Although this effect is attenuated when compared to *Dat*^{+/+} mice, the persistent presence of metabolic effects of cocaine in the brain of *Dat*-KO mice demonstrates that this phenomenon is partially dopamine-independent (Thanos et al., 2008).

An effect of chronic cocaine exposure on mitovesicle generation is also supported by the finding that numerous proteins were found at a lower level in mitovesicles isolated from cocaine-intoxicated brains when compared to controls (Figure 2a–e), suggesting a cocaine-dependent impairment of mitovesicle cargo loading during mitovesicle biogenesis. The amounts of several mitovesicle proteins were perturbed by cocaine in a sex-dependent fashion. In male mitovesicles, but not female, we found a selective reduction of VDAC (a carrier of small hydrophilic molecules, including pyruvate and other energy-producing molecules, across the OMM) and of ETC complex I/V subunits induced by the drug (Figure 2a–e), causing a functional alteration in the ATP production capacity of male mitovesicles (Figure 2f). Given that there were no differences in the levels of the same proteins in brain homogenates (Figure 2g–p) we concluded that the sex-specific impairments of mitovesicles were not due to the downregulation of the expression of cargo proteins within brain cells but were related exclusively to mitovesicle cargo loading.

Unlike males, females did not show any difference induced by cocaine in the energy production capacity of brain mitovesicles (Figure 2), suggesting a sex-dependent protective mechanism that restores, at least partially, the physiological mitochondrial activity and ATP production in the brain of female, but not male, individuals with cocaine use disorder. Unfortunately, the majority of data in the field are collected only from male subjects, and our data show that studies of the bioenergetic effects of cocaine on the brain of female subjects should be conducted. Although beyond the scope of this work, we hypothesise a role for testosterone in the findings presented here. It was shown that cocaine can increase the quantity of testosterone in the blood of female, but not male, rhesus monkeys and human subjects (Heesch et al., 1996; Mello et al., 2004; Mendelson et al., 2003). Testosterone is a positive master regulator of metabolism and has a protective function on brain mitochondria (Gaignard et al., 2017; Toro-Urrego et al., 2016; Yan et al., 2017; Yan et al., 2021). Thus, it is possible that the higher testosterone levels induced by cocaine boost oxidative phosphorylation and mitochondrial health in the brain of females but not males and partially avoid bioenergetic and cargo changes in mitovesicles.

A sex-independent effect of cocaine was found for MAO-A, levels of which were lower in mitovesicles isolated from the brain of both male and female treated mice compared to sex-matched saline controls (Figure 2b,c). This would result in higher

intracellular retention of MAO-A in both sexes. MAO-A is the main monoamine neurotransmitter-degrading enzyme in the brain (including dopamine) and is specifically expressed by dopaminergic and other monoaminergic neurones (Cho et al., 2021). It produces H_2O_2 as a byproduct (Cho et al., 2021), suggesting that an elevation in MAO-A intracellular levels as a consequence of its lower elimination from the cell via mitovesicles, can contribute to the toxic effects of cocaine on the monoaminergic system, both as a ROS-generating agent, and as a monoamine network modifier. Furthermore, mitovesicle-bound, extracellular MAO-A is enzymatically active (D'Acunzo et al., 2021), and can potentially alleviate the higher dopamine levels that accumulate in the brain extracellular space of individuals with cocaine use disorder due to DAT inhibition. Accordingly, monoaminergic neurones would benefit from a higher release of this enzyme from the cell. Thus, it is conceivable that the cocaine-dependent impairment in MAO-A loading onto the surface of mitovesicles is a previously unidentified mechanism by which cocaine exacerbates its action in the brain and should be explored as a novel therapeutic target for addiction intervention. Furthermore, these data suggest that mitovesicles and specifically MAO-A extracellular levels can be useful as biomarkers to assess the status of monoaminergic neurons during cocaine chronic exposure, and perhaps to monitor the restoration to normal levels during withdrawal/recover.

The hypothesis that mitovesicle exocytosis may act as a homeostatic mechanism to alleviate mitochondrial stress is consistent with earlier findings in other murine models of disease and physiological dysfunctions with mitochondrial abnormalities, including in aged mice when compared to younger counterparts (Kim et al., 2022). Furthermore, we previously found a similar correlation between brain hypometabolism, higher levels of mitovesicles, and a mitovesicle-specific downregulation in ETC complex subunits in a mouse model of Down syndrome (D'Acunzo et al., 2021; Zammit et al., 2020), indicating a similar complex and generalised interconnection between intracellular and extracellular pathways involved in mitochondrial quality control when the homeostasis is altered, regardless of the source of the insult. Thus, mitovesicles may be a previously unidentified player in the biology of cocaine addiction and therapies to fine tune brain mitovesicle functionality should be explored to restore normal metabolism and mitigate the effects of chronic cocaine exposure.

GEOLOCALIZATION INFORMATION

Center for Dementia Research, Nathan S. Kline Institute for Psychiatric Research, 140 Old Orangeburg Road, Orangeburg, NY 10962–1157, United States.

AUTHOR CONTRIBUTIONS

Pasquale D'Acunzo: Conceptualization; Data curation; Formal analysis; Investigation; Methodology; Project administration; Supervision; Validation; Visualization; Writing – original draft. Jonathan Ungania: Investigation. Yohan Kim: Data curation; Formal analysis; Investigation; Writing – review & editing. Bryana Barreto: Investigation. Steven DeRosa: Resources. Monika Pawlik: Resources; Writing – review & editing. Stefanie Canals-Baker: Investigation; Resources. Hediye Erdjument-Bromage: Data curation; Formal analysis; Investigation; Validation; Writing – original draft; Writing – review & editing. Audrey Hashim: Investigation; Resources. Chris Goulbourne: Investigation; Writing – review & editing. Thomas Neubert: Data curation; Funding acquisition; Supervision; Writing – review & editing. Mariko Saito: Funding acquisition; Project administration; Supervision; Writing – review & editing. Henry Sershen: Funding acquisition; Project administration; Supervision; Writing – review & editing. Efrat Levy: Conceptualization; Funding acquisition; Project administration; Supervision; Writing – original draft.












ACKNOWLEDGEMENTS

This work was supported by the National Institute on Drug Abuse (grant number DA044489 to E.L. and M.S.), the National Institute of Health Shared Instrumentation Program (grant number S10 RR027990 to T.A.N.), and the National Institute on Aging (grant number AG057517 to E.L.). We thank P. M. Mathews and L. Rachmany for discussions; X. Zhang, G. Zaghen, K. Smith, K. Casey, and A. Aroh for technical support; G. Ferrari for coordinating and managing our laboratory.

CONFLICT OF INTEREST

The authors report no competing interests.

ORCID

Pasquale D'Acunzo  <https://orcid.org/0000-0001-7237-0076>
 Jonathan M. Ungania  <https://orcid.org/0000-0003-3592-0846>
 Yohan Kim  <https://orcid.org/0000-0003-2550-8751>
 Bryana R. Barreto  <https://orcid.org/0000-0003-0631-9066>
 Monika Pawlik  <https://orcid.org/0000-0003-0138-7529>
 Hediye Erdjument-Bromage  <https://orcid.org/0000-0003-0224-3594>
 Chris N. Goulbourne  <https://orcid.org/0000-0003-1185-2682>
 Thomas A. Neubert  <https://orcid.org/0000-0001-7049-2088>
 Mariko Saito  <https://orcid.org/0000-0001-9383-4458>
 Henry Sershen  <https://orcid.org/0000-0002-7922-2217>
 Efrat Levy  <https://orcid.org/0000-0001-6890-6763>

REFERENCES

- Barreto, B. R., D'Acunzo, P., Ungania, J. M., Das, S., Hashim, A., Goulbourne, C. N., Canals-Baker, S., Saito, M., Saito, M., Serksen, H., & Levy, E. (2022). Cocaine modulates the neuronal endosomal system and extracellular vesicles in a sex-dependent manner. *Neurochemical Research*, 47(8), 2263–2277.
- Beatriz, M., Vilaça, R., Anjo, S. I., Manadas, B., Januário, C., Rego, A. C., & Lopes, C. (2022). Defective mitochondria-lysosomal axis enhances the release of extracellular vesicles containing mitochondrial DNA and proteins in Huntington's disease. *Journal of Extracellular Biology*, 1, e65.
- Bhattacharjee, A., Djekidel, M. N., Chen, R., Chen, W., Tuesta, L. M., & Zhang, Y. (2019). Cell type-specific transcriptional programs in mouse prefrontal cortex during adolescence and addiction. *Nature Communications*, 10, 4169.
- Block, E. R., Nuttle, J., Balcita-Pedicino, J. J., Caltagare, J., Watkins, S. C., Sesack, S. R., & Sorkin, A. (2015). Brain region-specific trafficking of the dopamine transporter. *Journal of Neuroscience*, 35, 12845–12858.
- Cave, J. W., & Baker, H. (2009). Dopamine systems in the forebrain. *Advances in Experimental Medicine and Biology*, 651, 15–35.
- Chandra, R., Engeln, M., Schiefer, C., Patton, M. H., Martin, J. A., Werner, C. T., Riggs, L. M., Francis, T. C., McGlincy, M., Evans, B., Nam, H., Das, S., Girven, K., Konkalmatt, P., Gancarz, A. M., Golden, S. A., Iniguez, S. D., Russo, S. J., Turecki, G., ... Lobo, M. K. (2017). Drp1 mitochondrial fission in D1 neurons mediates behavioral and cellular plasticity during early cocaine abstinence. *Neuron*, 96, 1327–1341. e1326.
- Cheung, Y. T., Lau, W. K., Yu, M. S., Lai, C. S., Yeung, S. C., So, K. F., & Chang, R. C. (2009). Effects of all-trans-retinoic acid on human SH-SY5Y neuroblastoma as in vitro model in neurotoxicity research. *Neurotoxicology*, 30, 127–135.
- Cho, H. U., Kim, S., Sim, J., Yang, S., An, H., Nam, M. H., Jang, D. P., & Lee, C. J. (2021). Redefining differential roles of MAO-A in dopamine degradation and MAO-B in tonic GABA synthesis. *Experimental & Molecular Medicine*, 53, 1148–1158.
- Ciliax, B. J., Drash, G. W., Staley, J. K., Haber, S., Mobley, C. J., Miller, G. W., Mufson, E. J., Mash, D. C., & Levey, A. I. (1999). Immunocytochemical localization of the dopamine transporter in human brain. *Journal of Comparative Neurology*, 409, 38–56.
- Cox, J., Neuhauser, N., Michalski, A., Scheltema, R. A., Olsen, J. V., & Mann, M. (2011). Andromeda: A peptide search engine integrated into the MaxQuant environment. *Journal of Proteome Research*, 10, 1794–1805.
- Crewe, C., Funcke, J. B., Li, S., Joffin, N., Gliniak, C. M., Ghaben, A. L., An, Y. A., Sadek, H. A., Gordillo, R., Akgul, Y., Chen, S., Samovski, D., Fischer-Posovszky, P., Kusminski, C. M., Klein, S., & Scherer, P. E. (2021). Extracellular vesicle-based interorgan transport of mitochondria from energetically stressed adipocytes. *Cell Metabolism*, 33, 1853–1868. e1811.
- Cunha-Oliveira, T., Rego, A. C., Cardoso, S. M., Borges, F., Swerdlow, R. H., Macedo, T., & de Oliveira, C. R. (2006). Mitochondrial dysfunction and caspase activation in rat cortical neurons treated with cocaine or amphetamine. *Brain Research*, 1089, 44–54.
- Cunha-Oliveira, T., Rego, A. C., Garrido, J., Borges, F., Macedo, T., & Oliveira, C. R. (2010). Neurotoxicity of heroin-cocaine combinations in rat cortical neurons. *Toxicology*, 276, 11–17.
- Cunha-Oliveira, T., Silva, L., Silva, A. M., Moreno, A. J., Oliveira, C. R., & Santos, M. S. (2013a). Mitochondrial complex I dysfunction induced by cocaine and cocaine plus morphine in brain and liver mitochondria. *Toxicology Letters*, 219, 298–306.
- Cunha-Oliveira, T., Silva, L., Silva, A. M., Moreno, A. J., Oliveira, C. R., & Santos, M. S. (2013b). Acute effects of cocaine, morphine and their combination on bioenergetic function and susceptibility to oxidative stress of rat liver mitochondria. *Life Sciences*, 92, 1157–1164.
- D'Acunzo, P., Hargash, T., Pawlik, M., Goulbourne, C. N., Perez-Gonzalez, R., & Levy, E. (2019). Enhanced generation of intraluminal vesicles in neuronal late endosomes in the brain of a Down syndrome mouse model with endosomal dysfunction. *Developmental Neurobiology*, 79, 656–663.
- D'Acunzo, P., Kim, Y., Ungania, J. M., Perez-Gonzalez, R., Goulbourne, C. N., & Levy, E. (2022). Isolation of mitochondria-derived mitovesicles and subpopulations of microvesicles and exosomes from brain tissues. *Nature Protocols*, 17, 2517–2549.
- D'Acunzo, P., Perez-Gonzalez, R., Kim, Y., Hargash, T., Miller, C., Alldred, M. J., Erdjument-Bromage, H., Penikalapati, S. C., Pawlik, M., Saito, M., Saito, M., Ginsberg, S. D., Neubert, T. A., Goulbourne, C. N., & Levy, E. (2021). Mitovesicles are a novel population of extracellular vesicles of mitochondrial origin altered in Down syndrome. *Science Advances*, 7, eabe5085.
- D'Acunzo, P., Strappazzon, F., Caruana, I., Meneghetti, G., Di Rita, A., Simula, L., Weber, G., Del Bufalo, F., Dalla Valle, L., Campello, S., Locatelli, F., & Cecconi, F. (2019). Reversible induction of mitophagy by an optogenetic bimodular system. *Nature Communications*, 10, 1533.
- De Simone, F. I., Darbinian, N., Amini, S., Muniswamy, M., White, M. K., Elrod, J. W., Datta, P. K., Langford, D., & Khalili, K. (2016). HIV-1 tat and cocaine impair survival of cultured primary neuronal cells via a mitochondrial pathway. *Journal of Neuroimmune Pharmacology*, 11, 358–368.
- Dietrich, J. B., Poirier, R., Aunis, D., & Zwiller, J. (2004). Cocaine downregulates the expression of the mitochondrial genome in rat brain. *Annals of the New York Academy of Sciences*, 1025, 345–350.
- Di Rita, A., Angelini, D. F., Maiorino, T., Caputo, V., Cascella, R., Kumar, M., Tiberti, M., Lambrugh, M., Wesch, N., Lohr, F., Dotsch, V., Carinci, M., D'Acunzo, P., Chiurciu, V., Papaleo, E., Rogov, V. V., Giardina, E., Battistini, L., & Strappazzon, F. (2021). Characterization of a natural variant of human NDP52 and its functional consequences on mitophagy. *Cell Death and Differentiation*, 28, 2499–2516.
- Di Rita, A., D'Acunzo, P., Simula, L., Campello, S., Strappazzon, F., & Cecconi, F. (2018). AMBRA1-mediated mitophagy counteracts oxidative stress and apoptosis induced by neurotoxicity in human neuroblastoma SH-SY5Y cells. *Frontiers in Cellular Neuroscience*, 12, 92.
- Di Rita, A., Peschiaroli, A., Acunzo, P. D., Strobbe, D., Hu, Z., Gruber, J., Nygaard, M., Lambrugh, M., Melino, G., Papaleo, E., Dengjel, J., El Alaoui, S., Campanella, M., Dotsch, V., Rogov, V. V., Strappazzon, F., & Cecconi, F. (2018). HUWE1 E3 ligase promotes PINK1/PARKIN-independent mitophagy by regulating AMBRA1 activation via IKKalpha. *Nature Communications*, 9, 3755.
- Erdjument-Bromage, H., Huang, F. K., & Neubert, T. A. (2018). Sample preparation for relative quantitation of proteins using tandem mass tags (TMT) and mass spectrometry (MS). *Methods in Molecular Biology*, 1741, 135–149.
- Fecher, C., Trovo, L., Muller, S. A., Snaidero, N., Wettmarshausen, J., Heink, S., Ortiz, O., Wagner, I., Kuhn, R., Hartmann, J., Karl, R. M., Konnerth, A., Korn, T., Wurst, W., Merkler, D., Lichtenthaler, S. F., Perocchi, F., & Miggel, T. (2019). Cell-type-specific profiling of brain mitochondria reveals functional and molecular diversity. *Nature Neuroscience*, 22, 1731–1742.
- Funakoshi, T., Furukawa, M., Aki, T., & Uemura, K. (2019). Repeated exposure of cocaine alters mitochondrial dynamics in mouse neuroblastoma Neuro2a. *Neurotoxicology*, 75, 70–77.
- Gagnard, P., Liere, P., Therond, P., Schumacher, M., Slama, A., & Guennoun, R. (2017). Role of sex hormones on brain mitochondrial function, with special reference to aging and neurodegenerative diseases. *Frontiers in Aging Neuroscience*, 9, 406.
- Gao, Q., Tian, R., Han, H., Slone, J., Wang, C., Ke, X., Zhang, T., Li, X., He, Y., Liao, P., Wang, F., Chen, Y., Fu, S., Zhang, K., Zeng, F., Yang, Y., Li, Z., Tan, J., Li, J., ... Zhang, Z. (2022). PINK1-mediated Drp1(S616) phosphorylation modulates synaptic development and plasticity via promoting mitochondrial fission. *Signal Transduction and Targeted Therapy*, 7, 103.

- Gauthier, S. A., Perez-Gonzalez, R., Sharma, A., Huang, F. K., Alldred, M. J., Pawlik, M., Kaur, G., Ginsberg, S. D., Neubert, T. A., & Levy, E. (2017). Enhanced exosome secretion in Down syndrome brain—A protective mechanism to alleviate neuronal endosomal abnormalities. *Acta Neuropathologica Communications*, 5, 65.
- He, J., Xiao, Y., Casiano, C. A., & Zhang, L. (2000). Role of mitochondrial cytochrome c in cocaine-induced apoptosis in coronary artery endothelial cells. *Journal of Pharmacology and Experimental Therapeutics*, 295, 896–903.
- Heesch, C. M., Negus, B. H., Bost, J. E., Keffer, J. H., Snyder, R. W. 2nd, & Eichhorn, E. J. (1996). Effects of cocaine on anterior pituitary and gonadal hormones. *Journal of Pharmacology and Experimental Therapeutics*, 278, 1195–1200.
- Heo, J. M., Ordureau, A., Paulo, J. A., Rinehart, J., & Harper, J. W. (2015). The PINK1-PARKIN mitochondrial ubiquitylation pathway drives a program of OPTN/NDP52 recruitment and TBK1 activation to promote mitophagy. *Molecular Cell*, 60, 7–20.
- Heo, J. M., Ordureau, A., Swarup, S., Paulo, J. A., Shen, K., Sabatini, D. M., & Harper, J. W. (2018). RAB7A phosphorylation by TBK1 promotes mitophagy via the PINK-PARKIN pathway. *Science Advances*, 4, eAav0443.
- Huang, F. K., Zhang, G., Lawlor, K., Nazarian, A., Philip, J., Tempst, P., Dephoure, N., & Neubert, T. A. (2017). Deep coverage of global protein expression and phosphorylation in breast tumor cell lines using TMT 10-plex isobaric labeling. *Journal of Proteome Research*, 16, 1121–1132.
- Jeppesen, D. K., Fenix, A. M., Franklin, J. L., Higginbotham, J. N., Zhang, Q., Zimmerman, L. J., Liebler, D. C., Ping, J., Liu, Q., Evans, R., Fissell, W. H., Patton, J. G., Rome, L. H., Burnette, D. T., & Coffey, R. J. (2019). Reassessment of exosome composition. *Cell*, 177, 428–445. e418.
- Kim, D. I., Lee, K. H., Gabr, A. A., Choi, G. E., Kim, J. S., Ko, S. H., & Han, H. J. (2016). Abeta-Induced Drp1 phosphorylation through Akt activation promotes excessive mitochondrial fission leading to neuronal apoptosis. *Biochimica Et Biophysica Acta*, 1863, 2820–2834.
- Kim, Y., Perez-Gonzalez, R., Miller, C., Kurz, M., D'Acunzo, P., Goulbourne, C. N., & Levy, E. (2022). Sex differentially alters secretion of brain extracellular vesicles during aging: A potential mechanism for maintaining brain homeostasis. *Neurochemical Research*, 47, 3428–343.
- Korshunov, S. S., Skulachev, V. P., & Starkov, A. A. (1997). High protonic potential actuates a mechanism of production of reactive oxygen species in mitochondria. *Febs Letters*, 416, 15–18.
- Landfield, Q., Saito, M., Hashim, A., Canals-Baker, S., Sershen, H., Levy, E., & Saito, M. (2021). Cocaine induces sex-associated changes in lipid profiles of brain extracellular vesicles. *Neurochemical Research*, 46, 2909–2922.
- Lehrmann, E., Oylar, J., Vawter, M. P., Hyde, T. M., Kolachana, B., Kleinman, J. E., Huestis, M. A., Becker, K. G., & Freed, W. J. (2003). Transcriptional profiling in the human prefrontal cortex: Evidence for two activation states associated with cocaine abuse. *Pharmacogenomics Journal*, 3, 27–40.
- Li, J., Lee, Y., Johansson, H. J., Mager, I., Vader, P., Nordin, J. Z., Wiklander, O. P., Lehtio, J., Wood, M. J., & Andaloussi, S. E. (2015). Serum-free culture alters the quantity and protein composition of neuroblastoma-derived extracellular vesicles. *Journal of Extracellular Vesicles*, 4, 26883.
- Linares, R., Tan, S., Gounou, C., & Brisson, A. R. (2017). Imaging and quantification of extracellular vesicles by transmission electron microscopy. *Methods in Molecular Biology*, 1545, 43–54.
- London, E. D., Cascella, N. G., Wong, D. F., Phillips, R. L., Dannals, R. F., Links, J. M., Herning, R., Grayson, R., Jaffe, J. H., & Wagner, H. N. Jr. (1990). Cocaine-induced reduction of glucose utilization in human brain. A study using positron emission tomography and [fluorine 18]-fluorodeoxyglucose. *Archives of General Psychiatry*, 47, 567–574.
- Luo, F., Herrup, K., Qi, X., & Yang, Y. (2017). Inhibition of Drp1 hyper-activation is protective in animal models of experimental multiple sclerosis. *Experimental Neurology*, 292, 21–34.
- Mash, D. C., French-Mullen, J., Adi, N., Qin, Y., Buck, A., & Pablo, J. (2007). Gene expression in human hippocampus from cocaine abusers identifies genes which regulate extracellular matrix remodeling. *PLoS ONE*, 2, e1187.
- Mello, N. K., Mendelson, J. H., Negus, S. S., Kelly, M., Knudson, I., & Roth, M. E. (2004). The effects of cocaine on gonadal steroid hormones and LH in male and female rhesus monkeys. *Neuropsychopharmacology*, 29, 2024–2034.
- Mendelson, J. H., Sholar, M. B., Mutschler, N. H., Jaszyna-Gasior, M., Goletiani, N. V., Siegel, A. J., & Mello, N. K. (2003). Effects of intravenous cocaine and cigarette smoking on luteinizing hormone, testosterone, and prolactin in men. *Journal of Pharmacology and Experimental Therapeutics*, 307, 339–348.
- Narendra, D., Tanaka, A., Suen, D. F., & Youle, R. J. (2008). Parkin is recruited selectively to impaired mitochondria and promotes their autophagy. *Journal of Cell Biology*, 183, 795–803.
- Narendra, D. P., Jin, S. M., Tanaka, A., Suen, D. F., Gautier, C. A., Shen, J., Cookson, M. R., & Youle, R. J. (2010). PINK1 is selectively stabilized on impaired mitochondria to activate Parkin. *Plos Biology*, 8, e1000298.
- Peng, K. Y., Perez-Gonzalez, R., Alldred, M. J., Goulbourne, C. N., Morales-Corraliza, J., Saito, M., Saito, M., Ginsberg, S. D., Mathews, P. M., & Levy, E. (2019). Apolipoprotein E4 genotype compromises brain exosome production. *Brain*, 142, 163–175.
- Phinney, D. G., Di Giuseppe, M., Njah, J., Sala, E., Shiva, S., St Croix, C. M., Stolz, D. B., Watkins, S. C., Di, Y. P., Leikauf, G. D., Kolls, J., Riches, D. W., Deiluiis, G., Kaminski, N., Boregowda, S. V., McKenna, D. H., & Ortiz, L. A. (2015). Mesenchymal stem cells use extracellular vesicles to outsource mitophagy and shuttle microRNAs. *Nature Communications*, 6, 8472.
- Picard, M., White, K., & Turnbull, D. M. (2013). Mitochondrial morphology, topology, and membrane interactions in skeletal muscle: A quantitative three-dimensional electron microscopy study. *Journal of Applied Physiology*, 114, 161–171.
- Picca, A., Guerra, F., Calvani, R., Coelho-Junior, H. J., Bossola, M., Landi, F., Bernabei, R., Bucci, C., & Marzetti, E. (2020). Generation and release of mitochondrial-derived vesicles in health, aging and disease. *Journal of Clinical Medicine*, 9, 1440.
- Puhm, F., Afonyushkin, T., Resch, U., Obermayer, G., Rohde, M., Penz, T., Schuster, M., Wagner, G., Rendeiro, A. F., Melki, I., Kaun, C., Wojta, J., Bock, C., Jilma, B., Mackman, N., Boilard, E., & Binder, C. J. (2019). Mitochondria are a subset of extracellular vesicles released by activated monocytes and induce type I IFN and TNF responses in endothelial cells. *Circulation Research*, 125, 43–52.
- Reith, M. E., Ali, S., Hashim, A., Sheikh, I. S., Theddu, N., Gaddiraju, N. V., Mehrotra, S., Schmitt, K. C., Murray, T. F., Sershen, H., Unterwald, E. M., & Davis, F. A. (2012). Novel C-1 substituted cocaine analogs unlike cocaine or benztropine. *Journal of Pharmacology and Experimental Therapeutics*, 343, 413–425.
- Richter, B., Sliter, D. A., Herhaus, L., Stolz, A., Wang, C., Beli, P., Zaffagnini, G., Wild, P., Martens, S., Wagner, S. A., Youle, R. J., & Dikic, I. (2016). Phosphorylation of OPTN by TBK1 enhances its binding to Ub chains and promotes selective autophagy of damaged mitochondria. *PNAS*, 113, 4039–4044.
- Roe, A. J., & Qi, X. (2018). Drp1 phosphorylation by MAPK1 causes mitochondrial dysfunction in cell culture model of Huntington's disease. *Biochemical and Biophysical Research Communications*, 496, 706–711.
- Romach, M. K., Glue, P., Kampman, K., Kaplan, H. L., Somer, G. R., Poole, S., Clarke, L., Coffin, V., Cornish, J., O'Brien, C. P., & Sellers, E. M. (1999). Attenuation of the euphoric effects of cocaine by the dopamine D1/D5 antagonist ecopipam (SCH 39166). *Archives of General Psychiatry*, 56, 1101–1106.
- Rosina, M., Ceci, V., Turchi, R., Chuan, L., Borchering, N., Sciarretta, F., Sanchez-Diaz, M., Tortolici, F., Karlinsey, K., Chiurciu, V., Fuoco, C., Giwa, R., Field, R. L., Audano, M., Arena, S., Palma, A., Riccio, F., Shamsi, F., Renzone, G., ... Lettieri-Barbato, D. (2022). Ejection of damaged mitochondria and their removal by macrophages ensure efficient thermogenesis in brown adipose tissue. *Cell metabolism*, 34, 533–548. e512.
- Schneider, C. A., Rasband, W. S., & Eliceiri, K. W. (2012). NIH Image to ImageJ: 25 years of image analysis. *Nature Methods*, 9, 671–675.

- Sugiura, A., McLelland, G. L., Fon, E. A., & McBride, H. M. (2014). A new pathway for mitochondrial quality control: Mitochondrial-derived vesicles. *Embo Journal*, 33, 2142–2156.
- Thangaraj, A., Periyasamy, P., Guo, M. L., Chivero, E. T., Callen, S., & Buch, S. (2020). Mitigation of cocaine-mediated mitochondrial damage, defective mitophagy and microglial activation by superoxide dismutase mimetics. *Autophagy*, 16, 289–312.
- Thanos, P. K., Michaelides, M., Benveniste, H., Wang, G. J., & Volkow, N. D. (2008). The effects of cocaine on regional brain glucose metabolism is attenuated in dopamine transporter knockout mice. *Synapse*, 62, 319–324.
- Thery, C., Witwer, K. W., Aikawa, E., Alcaraz, M. J., Anderson, J. D., Andriantsitohaina, R., Antoniou, A., Arab, T., Archer, F., Atkin-Smith, G. K., Ayre, D. C., Bach, J. M., Bachurski, D., Baharvand, H., Balaj, L., Baldacchino, S., Bauer, N. N., Baxter, A. A., Bebawy, M., ... Zuba-Surma, E. K. (2018). Minimal information for studies of extracellular vesicles 2018 (MISEV2018): A position statement of the International Society for Extracellular Vesicles and update of the MISEV2014 guidelines. *Journal of Extracellular Vesicles*, 7, 1535750.
- Thornton, C., Grad, E., & Yaka, R. (2021). The role of mitochondria in cocaine addiction. *Biochemical Journal*, 478, 749–764.
- Tomaipitina, L., Petrunaro, S., D'Acunzo, P., Facchiano, A., Dubey, A., Rizza, S., Giulitti, F., Gaudio, E., Filippini, A., Ziparo, E., Cecconi, F., & Giampietri, C. (2021). c-FLIP regulates autophagy by interacting with Beclin-1 and influencing its stability. *Cell Death & Disease*, 12, 686.
- Toro-Urrego, N., Garcia-Segura, L. M., Echeverria, V., & Barreto, G. E. (2016). Testosterone protects mitochondrial function and regulates neuroglobin expression in astrocytic cells exposed to glucose deprivation. *Frontiers in Aging Neuroscience*, 8, 152.
- Turiault, M., Parnaudeau, S., Milet, A., Parlato, R., Rouzeau, J. D., Lazar, M., & Tronche, F. (2007). Analysis of dopamine transporter gene expression pattern – generation of DAT-iCre transgenic mice. *Febs Journal*, 274, 3568–3577.
- Tyanova, S., Temu, T., & Cox, J. (2016). The MaxQuant computational platform for mass spectrometry-based shotgun proteomics. *Nature Protocols*, 11, 2301–2319.
- Tyanova, S., Temu, T., Sinitcyn, P., Carlson, A., Hein, M. Y., Geiger, T., Mann, M., & Cox, J. (2016). The Perseus computational platform for comprehensive analysis of (prote)omics data. *Nature Methods*, 13, 731–740.
- Villen, J., & Gygi, S. P. (2008). The SCX/IMAC enrichment approach for global phosphorylation analysis by mass spectrometry. *Nature Protocols*, 3, 1630–1638.
- Volkow, N. D., Hitzemann, R., Wang, G. J., Fowler, J. S., Wolf, A. P., Dewey, S. L., & Handlesman, L. (1992). Long-term frontal brain metabolic changes in cocaine abusers. *Synapse*, 11, 184–190.
- Volkow, N. D., Wang, G. J., Fowler, J. S., Hitzemann, R., Angrist, B., Gatley, S. J., Logan, J., Ding, Y. S., & Pappas, N. (1999). Association of methylphenidate-induced craving with changes in right striato-orbitofrontal metabolism in cocaine abusers: Implications in addiction. *American Journal of Psychiatry*, 156, 19–26.
- Wang, X., Ryu, D., Houtkooper, R. H., & Auwerx, J. (2015). Antibiotic use and abuse: A threat to mitochondria and chloroplasts with impact on research, health, and environment. *Bioessays*, 37, 1045–1053.
- Wen, S., Aki, T., Funakoshi, T., Unuma, K., & Uemura, K. (2022). Role of mitochondrial dynamics in cocaine's neurotoxicity. *International Journal of Molecular Sciences*, 23, 5418.
- Wiemerslage, L., & Lee, D. (2016). Quantification of mitochondrial morphology in neurites of dopaminergic neurons using multiple parameters. *Journal of Neuroscience Methods*, 262, 56–65.
- Yan, W., Kang, Y., Ji, X., Li, S., Li, Y., Zhang, G., Cui, H., & Shi, G. (2017). Testosterone upregulates the expression of mitochondrial ND1 and ND4 and alleviates the oxidative damage to the nigrostriatal dopaminergic system in orchietomized rats. *Oxidative Medicine and Cellular Longevity*, 2017, 1202459.
- Yan, W., Zhang, T., Kang, Y., Zhang, G., Ji, X., Feng, X., & Shi, G. (2021). Testosterone ameliorates age-related brain mitochondrial dysfunction. *Aging (Albany NY)*, 13, 16229–16247.
- Yuan, C., & Acosta, D. Jr. (2000). Effect of cocaine on mitochondrial electron transport chain evaluated in primary cultures of neonatal rat myocardial cells and in isolated mitochondrial preparations. *Drug and Chemical Toxicology*, 23, 339–348.
- Zaidi, N., Maurer, A., Niek, S., & Kalbacher, H. (2008). Cathepsin D: A cellular roadmap. *Biochemical and Biophysical Research Communications*, 376, 5–9.
- Zammit, M. D., Laymon, C. M., Tudorascu, D. L., Hartley, S. L., Piro-Gambetti, B., Johnson, S. C., Stone, C. K., Mathis, C. A., Zaman, S. H., Klunk, W. E., Handen, B. L., Cohen, A. D., & Christian, B. T. (2020). Patterns of glucose hypometabolism in Down syndrome resemble sporadic Alzheimer's disease except for the putamen. *Alzheimers Dement (Amst)*, 12, e12138.
- Zhang, L., Elmer, L. W., & Little, K. Y. (1998). Expression and regulation of the human dopamine transporter in a neuronal cell line. *Brain Research Molecular Brain Research*, 59, 66–73.
- Zhang, Y., Varela, L., Szigeti-Buck, K., Williams, A., Stojkovic, M., Sestan-Pesa, M., Henao-Mejia, J., D'Acunzo, P., Levy, E., Flavell, R. A., Horvath, T. L., & Kaczmarek, L. K. (2021). Cerebellar Kv3.3 potassium channels activate TANK-binding kinase 1 to regulate trafficking of the cell survival protein Hax-1. *Nature Communications*, 12, 1731.
- Zhou, Z., Yuan, Q., Mash, D. C., & Goldman, D. (2011). Substance-specific and shared transcription and epigenetic changes in the human hippocampus chronically exposed to cocaine and alcohol. *PNAS*, 108, 6626–6631.

SUPPORTING INFORMATION

Additional supporting information can be found online in the Supporting Information section at the end of this article.

How to cite this article: D'Acunzo, P., Ungania, J. M., Kim, Y., Barreto, B. R., DeRosa, S., Pawlik, M., Canals-Baker, S., Erdjument-Bromage, H., Hashim, A., Goulbourne, C. N., Neubert, T. A., Saito, M., Sershen, H., & Levy, E. (2023). Cocaine perturbs mitovesicle biology in the brain. *Journal of Extracellular Vesicles*, 12, e12301. <https://doi.org/10.1002/jev2.12301>